# Contents

# Chapter 1

# Introduction

## 1.1 What are astroparticles?

Astroparticles (AP) are particles (atomic nuclei, electrons, photons, neutrinos, etc) arriving at the top of the Earth's atmosphere from space. These particles could have widely different energies, from $10^{-6}$ eV (photons in the radio band) up to $10^{20}$ eV (Ultra-High-Energy Cosmic Rays, UHECR). The maximal astroparticle energy scale is some $\sim 7$ orders of magnitudes higher than the energy scale of high-energy particle physics experiments like the Large Hadron Collider (LHC), $\sim 10$ TeV$= 10^{13}$ eV.

High energy particles produced in astronomical sources interact with matter in interstellar and intergalactic space, in the interplanetary medium and with the Earth atmosphere during their travel from the source to the detector on Earth. Trajectories of charged particles are affected by cosmic magnetic fields.

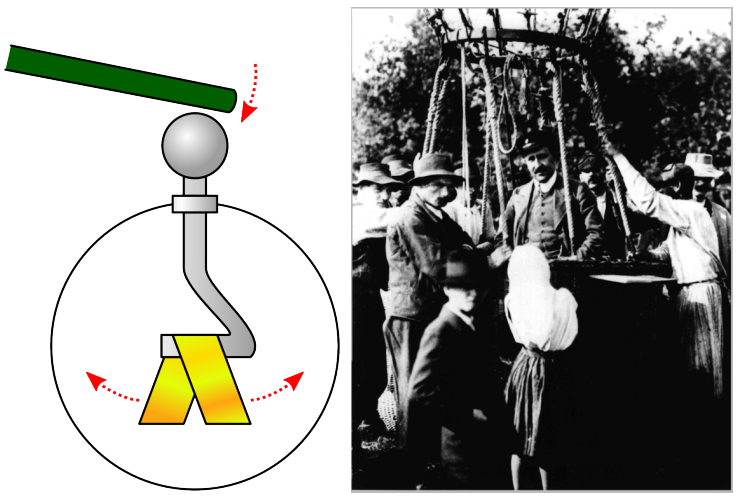

Figure 1.1.1: Left: Principle of operation of an electroscope. Right: Balloon flight of V.Hess, who made measurements of dependence of the rate of discharge of electroscope on the altitude, which led to the discovery of cosmic rays.

The history of Astroparticle physics started in 1912 with the discovery of cosmic rays by V.Hess. Today it is known that the cosmic rays discovered by Hess are atomic nuclei accelerated to high energies $E \gg m_p c^2$.

The first indications for existence of cosmic rays were obtained via measurements of dependence of ionization of air atoms with altitude. Such measurements were done by carrying an electroscope (a device which measures the rate of dis-

charge of an electrically charged body, see Fig. 1.1.1) on a balloon. At the beginning of 20th century it was known that the air close to the ground is ionized due to the radioactivity of the Earth (ground) and the initial idea was to verify that the level of ionization of the air would decrease with the increase of the altitude. This idea was behind the first balloon flights done by a swiss geophysicist A.Gockel, who discovered (1910) that the air ionization increases, rather than decreases with the increase of the altitude. Subsequent balloon flights by Hess and Köhlhorster (1911-1913) have proven that the hypothesis about the irradiation of the atmosphere by high-energy particles from space ("Höhenstrahlung") was correct one.

100 years after the discovery of cosmic rays the study of cosmic rays remains a research subject. It is known today that bulk of the particles irradiating the atmosphere are high-energy atomic nuclei with energies up to $10^{20}$ eV, see Fig. 1.2.1. Sub-dominant contributions to the cosmic ray flux are given by electrons, positrons (Fig. 1.2.2) and other particles. Direct detection of cosmic ray particles, study of their characteristics is possible using the high altitude balloon flights or sattellites (such as CREAM, AMS-02, Fig. 1.2.4). The sources of cosmic rays are unknown up to now and the "problem of the origin of cosmic rays" remains one of the major problems of Astroparticle Physics.

## 1.2 Astroparticle Physics

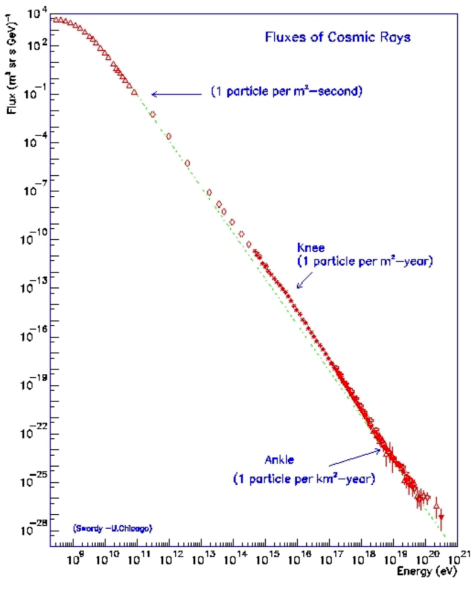


Figure 1.2.1: Spectrum of cosmic rays.

Astroparticle physics studies physical phenomena related to production, propagation and detection of astroparticles. High energy particles could be produced in astronomical objects such as neutron stars, black holes, supernovae, active and normal galaxies or galaxy clusters. Therefore, understanding of the processes of acceleration and propagation of astroparticles involves understanding of the physical conditions in these astronomical objects. In this respect Astroparticle physics is related to Astronomy. Interactions of high-energy particles take place also in the Early Universe. Astroparticles could also be produced in sources at cosmological distances. They cross significant part of the Universe before reaching the detector on Earth. In this respect Astroparticle Physics is related to Cosmology. Physical processes which lead to production of astroparticles in astronomical objects involve interactions between high-energy particles. Understanding of these phenomena is based on the knowledge of particle interactions in laboratory conditions studied at particle colliders, a research subject linking Astroparticle physics to high-energy physics.

High-energy particle physics studies fundamental constituents of matter: interactions of quarks

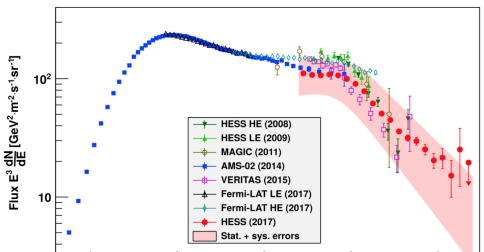

and leptons. Typical distance scales of such interactions are given by the Compton wavelength of a particle:

$$\lambda = \frac{\hbar}{mc} \simeq 3 \times 10^{-14} \left[\frac{m_p}{m}\right] \text{ cm} \qquad (1.2.1)$$

where $m$ is particle mass ($m_p$ is proton mass), $\hbar$ is the Planck constant and $c$ is the speed of light. For electron

$$m_e \simeq \frac{m_p}{1835} \qquad (1.2.2)$$

the Compton wavelength is $\lambda_e \simeq 10^{-10}$ cm. The time scale of particle interactions is estimated as

$$\tau \simeq \frac{\lambda}{c} \simeq 10^{-24} \left[\frac{m_p}{m}\right] \text{ s} \qquad (1.2.3)$$

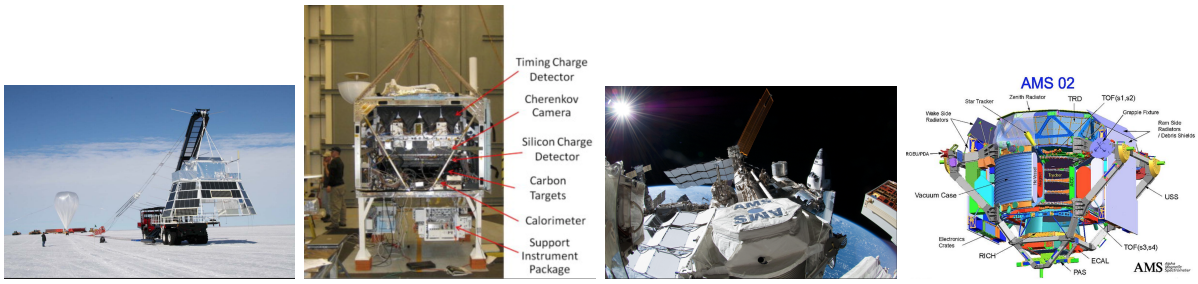


Figure 1.2.4: Cosmic ray detectors on a balloon (CREAM, two left panels) and spacecraft (AMS-02, two right panels).

The subject of Astronomy is the study of the properties of matter at very large distance scales, of the order from the size of stars

$$R_\odot \simeq 10^{11} \text{ cm} \qquad (1.2.4)$$

(the symbol $\odot$ means "the Sun") up to the size of the visible part of the Universe

$$R_H = \frac{c}{H_0} = \frac{3 \times 10^{10} \text{cm/s}}{70 \text{ km/s/Mpc}} \simeq 10^{28} \text{ cm} \simeq (several) \text{ Gpc} \qquad (1.2.5)$$

($H_0$ is the Hubble "constant", 1 pc= $3 \times 10^{18}$ cm is length unit in astronomy, parsec). Time scales associated to the cosmological distance scale is

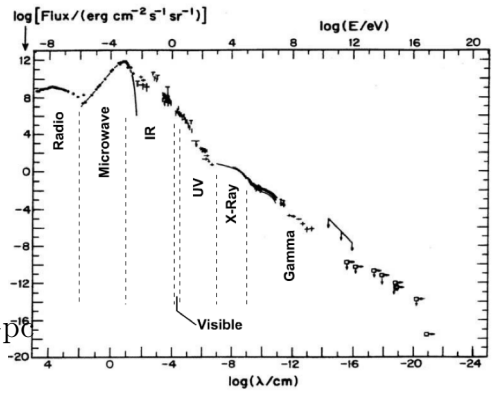


Figure 1.2.3: Spectrum of cosmic electromagnetic radiation.

$$T_H \simeq \frac{R_H}{c} \sim 3 \times 10^{17} \ s \sim 10 \text{ Gyr} \qquad (1.2.6)$$

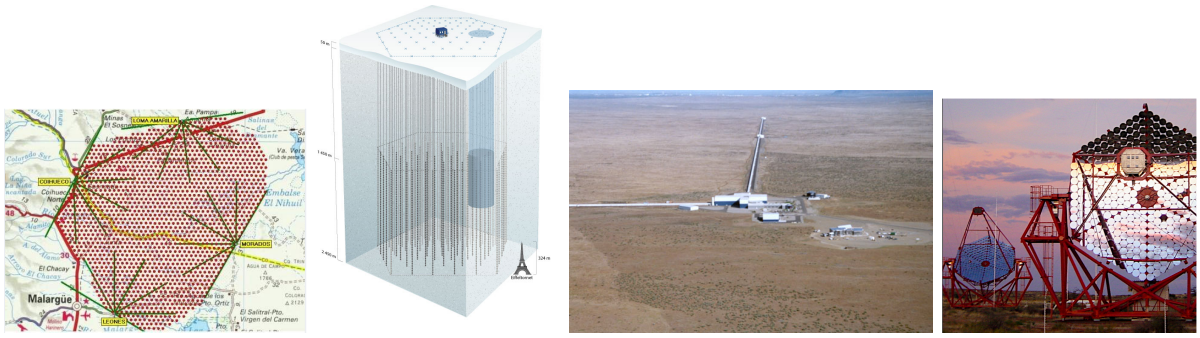


Figure 1.2.6: From left to right: Pierre Auger Observatory layout overlaid on the map of Malargue province in Argentina; IceCube neutrino telescope at the South Pole; gravitational wave detector LIGO. Length of the interferometer arm is $\sim 3$ km. HESS gamma-ray telescopes in Namibia.

Astroparticle physics relates the physics on the smallest and largest known time and distance scales.

Research methods conventionally used in astronomy and high-energy particle are very different. The main research tools of high-energy physicists are particle colliders, like e.g. the Large Hadron Collider (LHC) at CERN. The main research tool of an astronomer is a telescope (situated on the ground or in space). Research in Astroparticle physics involves research tools of both high-energy physics and astronomy.

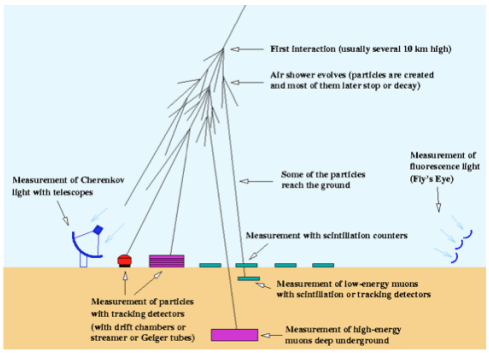


Figure 1.2.5: Methods of detection of astroparticles.

Interconnection between particle physics and astronomy (astrophysics) manifests itself in a variety of Astroparticle research sub-fields. In some cases these sub-fields are considered as parts of conventional "particle physics" research (i.e. scientists involved in research consider themselves as high-energy physicists), while in other cases the research is considered as a part of astronomy (i.e. researchers consider themselves as "astrophysicists"):

## 1.3 Astroparticle instrumentation

A wealth of astroparticle experimental facilities are currently taking data across the globe. A list (non-exhaustive) below gives some illustrative examples

- Pierre Auger Observatory (PAO) and Telescope Array (TA) are experiments for detection of Ultra-High-Energy Cosmic Rays (UHECR), which are particles with energies $E \sim 10^{20}$ eV. These are arrays of particle detectors (tanks filled with water and detecting Cherenkov radiation produced by secondary high-energy particles penetrating in the tanks in PAO). The detectors are scattered over an area up to

3000 km$^2$. Fig. 1.2.6 shows the layout of the PAO array, with each red point representing a water tank. In addition to the set surface particle detectors, PAO could detect UHECR with "fluorescence telescopes", which detect UV fluorescence emission produced by the air molecules exited by the secondary high-energy particles in the UHECR induced particle cascade in the atmosphere. The fields of view of the fluorescence telescopes of PAO are shown by green lines in Fig. 1.2.6.

- Very-High-Energy neutrino telescopes (IceCube, Fig. 1.2.6) are particle detectors using large volumes of water or ice with volumes up to $\sim$ 1 km$^3$ as the detection medium. They detect Cherenkov radiation emitted by high-energy muons produced in interactions of neutrinos crossing the body of the Earth. The largest VHE neutrino detector is currently IceCube neutrino telescope situated at the geographical South Pole.

- Graviational wave detectors, which are giant interferometers (with several km baselines) like LIGO detector, Fig. 1.2.6.

- Underground detectors. Detectors for the search of "rare" or extremely weakly interacting "dark matter" particles XENON, LUX and others. Neutrino detectors SuperKAMIOKANDE, SNO and others.

- Gamma-ray telescopes on the ground also use atmosphere as the detection medium. They detect Cherenkov radiation emitted by secondary high-energy particles produced in interactions of very-high-energy $\gamma$-rays in the atmosphere (HESS-II, MAGIC-II, VERITAS, CTA), Fig. 1.2.6.

- Space-based gamma-ray telescopes for direct detection of gamma-ray in the energy range 0.1 MeV-100 GeV *INTEGRAL, Fermi, AGILE*, Fig. 1.3.1.

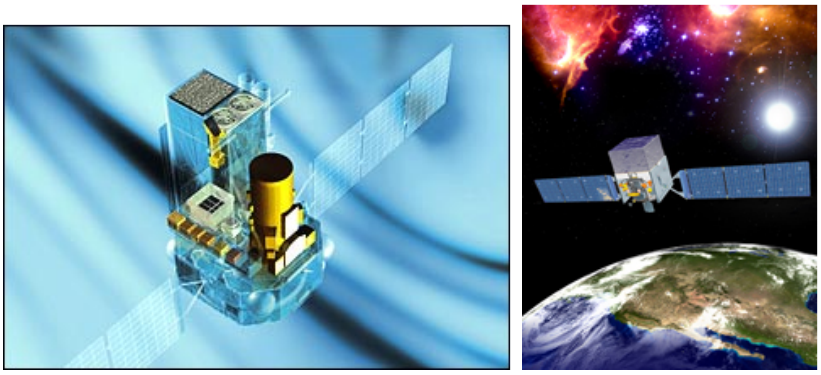

Figure 1.3.1: Space-based gamma-ray telescopes INTEGRAL (detects gamma-rays with energies below 1 MeV) and Fermi (GeV gamma-rays).

# Chapter 2

# Particle physics in the Early Universe

The average kinetic energy of particles in the room around us is $E_{kin} \sim T \sim 300$ K$\sim 10^{-1}$ eV. The energy is lower than the the binding energy of hydrogen atom, $E_H \simeq 15$ eV, and is much lower than the rest energy of electron, $E_e \simeq 5 \times 10^5$ eV. This means that the typical energy transfer in collisions of particles in the room is not sufficient to ionize the atoms or to produce electron-positron pairs or something even more exotic. This was not always the case, because the universe was hotter in the past. This part of the course considers the "thermal history" of cooling of our Universe.

## 2.1 Hubble law. Friedman equation.

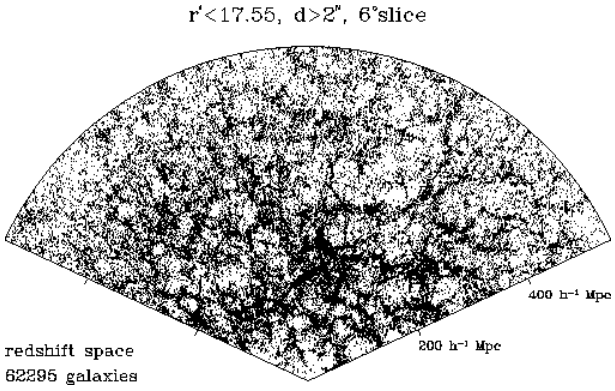


Figure 2.1.1: Distribution of galaxies observed by the Sloan Digital Sky Survey.

Back in 1929 E.Hubble has observed a phenomenon of systematic redshift of atomic spectral lines emitted by distant galaxies. The frequency of atomic lines decreased as $\nu = \nu_0/(1+z)$ where $z$, the redshift parameter, increased proportionally to the distance to a galaxy. This observation, interpreted as being due to the Doppler effect, shows that other galaxies escape away from the Milky Way with velocity $v \simeq zc$ (for small $z$). Hubble has found a relation between the velocity $v$ and the distance $r$

$$v = H_0 r \qquad (2.1.1)$$

The above relation is called "Hubble's law" and the proportionality coefficient in this relation $H_0$ is called "the Hubble constant".

The most natural interpretation of the Hubble's law is that the Universe around us expands. A popular analogy is with a yeast dough (=space) filled with raisins (=galaxies), which grows in volume when put in a warm place. When the dough expands, the distance between the raisins grows with the speed proportional to the distance.

Mathematical description of the expansion of the Universe is based on a hypothesis that all the matter is distributed homogeneously and isotropically all over the space, with average density $\rho$.

To describe expansion of a homogeneous and isotropic matter distribution, one can choose a reference frame with the origin at an arbitrary point and with an arbitrary orientation of the coordinate axes (the equations describing the expansion should not depend on the choice of the origin and orientation of the coordinate system). Next one considers dynamics of a small mass element $m$ at a distance $R$ at the time $t$. The mass contained inside the sphere is $M = (4\pi/3)\rho R^3$ ($\rho$ is the density of matter which is only the function of time in the homogeneous Universe). The energy conservation law for a particle on the surface of the sphere has the form

$$E = \frac{m\dot{R}^2}{2} - \frac{GmM}{R} = const \tag{2.1.2}$$

where $E$ is the total energy which is conserved. Dividing by $R^2$ gives Friedman equation

$$H^2 + \frac{k}{R^2} = \frac{8\pi G\rho}{3} \tag{2.1.3}$$

where $k = 2E/m$ and

$$H = \frac{\dot{R}}{R} \tag{2.1.4}$$

The parameter $H$ is called the "Hubble parameter". Its present day value $H_0$ is given in Eq. (**??**).

A proper description of the dynamics of the Universe should be done within a relativistic theory of gravity (this could be easily understood, because the Hubble law (2.1.1) implies that the escape velocity $v$ becomes comparable to the speed of light $v \sim c$ at a certain distance scale).

## 2.2 Matter equation of state.

Friedman equation (2.1.3) relates two functions of time, $R(t)$ and $\rho(t)$. To determine the time evolution of $R$ and $\rho$ one needs two equations, rather than just one. To find an additional equation involving $R$ and $\rho$, one could write the first law of Thermodynamics. The entire Universe is a closed thermodynamical system for which the 1-st law of Thermodynamics reads

$$dE = -pdV \tag{2.2.1}$$

where $E = (4\pi/3)\rho R^3$ is the total energy and $V = (4\pi/3)R^3$ is the volume. The pressure $p$ is conventionally related to $\rho$ via an "equation of state". In the most simple case(s), the equation of state has the form of a simple proportionality law

$$p = w\rho \tag{2.2.2}$$

The equation of state of the ideal gas $p = nT = (T/m)\rho$ where $m$ is the mass of the gas particles. For photon gas forming black body radiation $p = \rho/3$.

Substituting (2.2.2) into (2.2.1) one finds

$$\dot{\rho} = -3H\rho(1+w) \tag{2.2.3}$$

In the relativistic description of dynamics of the Universe, the right hand side of Eq. (2.1.3) could contain also a constant term,

$$H^2 + \frac{k}{R^2} = \frac{8\pi G}{3}\rho + \Lambda \tag{2.2.4}$$

$\Lambda$ is called the "cosmological constant". Introduction of $\Lambda$ is equivalent to the introduction of a new type of matter with the density $\rho_\Lambda = \Lambda/8\pi G$ and equation of state $w = -1$.

**Problem 1.** Solve the system of equations (2.2.3), (2.2.4) for $\Lambda = 0, k = 0$, assuming that the energy density $\rho \sim T^4$ is dominated by relativistic particle gas with temperature $T$ (e.g. photon gas) for which $w = 1/3$. Find the exponent $\kappa$ of the time evolution of the temperature $T(t) \propto t^{-\kappa}$.

## 2.3 Critical density. Dark Matter.

The present day rate of expansion of the Universe is

$$H(t_0) = H_0 \simeq 70 \frac{\text{Mpc}}{\text{km s}} \tag{2.3.1}$$

Eq. (2.1.3) defines a "characteristic" density scale of the Universe

$$\rho_0 = \frac{3H_0^2}{8\pi G} \simeq 10^{-29}\ \text{g/cm}^3 \tag{2.3.2}$$

If $\rho = \rho_c$ $k = 0$, i.e. $E = 0$ and the Universe is in a state which is a borderline between bound ($E < 0$ and unbound $E > 0$ state.

The density (2.3.2) is extremely small. For comparison, our average density is that of water, i.e. $\rho_{\text{human}} \simeq 1\ \text{g/cm}^3$. The density of the air at the bottom of the Earth atmosphere is $\rho_{\text{air}} \sim 10^{-3}\ \text{g/cm}^3$. The density (2.3.2) corresponds to $\sim 10^{-5}$ atoms of hydrogen per $\text{cm}^3$. However, it turns out that even this tiny density scale is difficult to explain based on our knowledge of the surrounding Universe.

A way to estimate the real density of the Universe around us it to measure the masses of galaxies (e.g. by counting the stars in the galaxies and adding the estimated masses of all the stars together), then estimate the number of galaxies per unit volume and then sum the masses of all galaxies in the unit volume. Doing such an estimate the astronomers arrive at a number

$$\rho_{\text{luminous}} = \Omega_{\text{luminous}}\rho_0,\ \Omega_{\text{luminous}} \simeq 10^{-2} \tag{2.3.3}$$

which is by a factor of $1/\Omega_{\text{luminous}} \sim 100$ smaller than the estimate obtained from the expansion rate of the Universe (2.3.2).

The discrepancy between the average density of the luminous matter and the total matter density of the Universe estimated from the expansion rate constitutes one of the major problems of modern physics, called the "Dark Matter" problem. It is well possible

that some amount of matter in the Universe does not emit enough light to be detected by the telescopes on the Earth. For example, there might be "dead" stars which do not emit light because their temperature is not enough to support the reactions of nuclear fusion. The Universe might also be full of "cold" bodies, like planets, which do not have intrinsic heat sources. There might be diffuse low density clouds of gas which were never heated to the temperatures high enough to be visible in the telescopes. In this case the "Dark Matter" might be one of the conventional forms of matter, known to us, but just not emitting light. It appears that this hypothesis does not work. The amount of cold conventional (often called "baryonic", because it is composed of atoms which contain baryons: protons and neutrons) matter in the Universe could be constrained by available observational data. This amount is not enough to explain the density scale of the Universe (2.3.2). This implies that there exists an unknown form of matter which dominates (by the overall mass) the Universe. One of the main challenges of Astroparticle physics is to clarify the nature of the Dark Matter.

## 2.4 Thermal history of the Universe

To understand what could be the Dark Matter which fills the Universe around us, we might try to understand where could this unknown form of matter come from. Our Universe is in a dynamical state of expansion, and physical conditions in the Universe in the past were different from the physical conditions in galaxies and in the intergalactic medium today. It is possible that the Dark Matter was not "dark" in the past in the sense that it was in contact with the known matter.

Observations in the microwave band (photon wavelengths $\lambda \sim 1$ mm, photon energies $h\nu \sim 10^{-4} - 10^{-3}$ eV) reveal the existence of an isotropic "background" radiation with thermal spectrum with temperature $T_0 \simeq 2.7$ K. The Cosmic Microwave Background (CMB) radiation is almost perfectly isotropic (the intensity of this radiation is the same in all directions on the sky, down to the level of $10^{-3}$) and has almost perfectly thermal spectrum. The present day density of CMB is $\rho_{\rm CMB} \simeq 0.25\,(T/2.7K)^4$ eV/cm$^3 \simeq 10^{-4}\rho_0$.

The expansion of the Universe dilutes the density of the CMB. Taking into account the equation of state of the gas of relativistic particles (photons), $w = 1/3$, one could find from Eq. (2.2.3) that the density of CMB decreases as $\rho_{\rm CMB} \sim R^{-4}$. The energy density of the photon gas is $\rho_{\rm CMB} \sim T^4$ which implies that the CMB was hotter in he past:

$$T \simeq 2.7\frac{R_0}{R}\ \text{K} \tag{2.4.1}$$

where $R_0$ is the present-day size (scale factor) of the Universe.

The temperature of the CMB was of the order of the temperature at the surface of the Sun ($T_\odot \simeq 5 \times 10^3$ K) when the Universe had the size (scale factor) $R/R_0 \sim 10^{-3}$. Physical processes relevant for the description of matter in the Universe at that moment were quite different from the processes relevant for the description of the Universe today. The Universe physical state was resembling that of a star.

At the temperature $T \sim 10^4$ K$\sim 10$ eV, thermal collisions between atoms lead to their ionization so that the matter is composed of charged ions and electrons, rather than

of atoms. In other words, the matter is in the form of an ionized plasma. The atoms could have formed only later than the matter-radiation equality moment, during the period called "recombination". At the moment of recombination, the rate of ionization in thermal collisions between plasma particles became small enough to allow hydrogen atoms to form and then not to be broken in collisions with photons. In other words, the reaction

$$H + \gamma \leftrightarrow p + e \tag{2.4.2}$$

should have fallen out of equilibrium, and proceeded only in the left-hand direction, with the right-hand direction being inefficient. The moment of recombination is one of the phase transitions which occurred in the past history of the Universe when it was cooling from high temperatures to the lower. There were several such phase transitions at still higher temperatures.

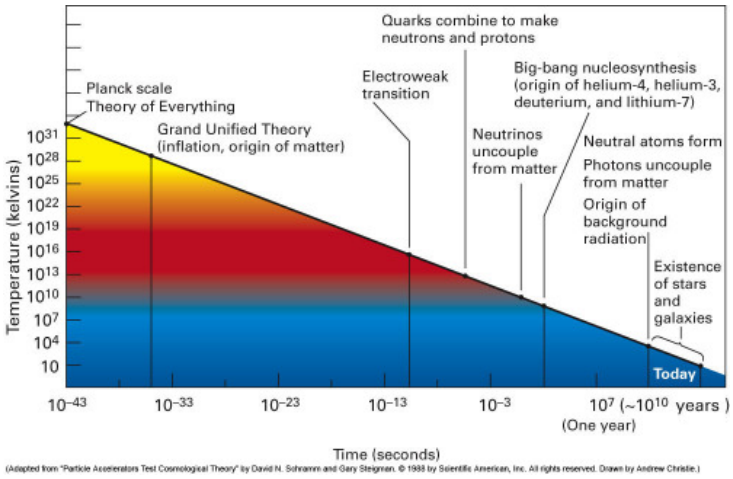


Figure 2.4.1: Thermal history of the Universe.

If one moves further back in time, one finds that the Universe was still more and more hot. For any temperature scale, one could find a moment of time when the temperature of the Universe was of the order of the given temperature scale. Rising temperature implies rising energy scale in particle collisions. Rising energy scales lead to "opening" of the new channels of particle interactions and, respectively, new phase transitions (from atoms to ionized plasma composed of atomic nuclei and electrons, from atomic nuclei to the gas of protons and neutrons, from protons and neutrons to quarks and gluons etc). Using our knowledge of the laws of physics at different energy scales, one could describe the "thermal history" of the Universe as shown in Fig. 2.4.1.

**Problem 2.** The energy density of CMB is a small fraction of the overall density estimated as $\rho_0$ composed of the dark matter (with density $\rho_{DM} \simeq 0.3\rho_0$ and equation of state $w \simeq 0$ and/or dark energy ($\rho_{DE} \simeq 0.7\rho_0$ and $w \simeq -1$).
Find the values of the scale factor $(R/R_0)$ back in time at which
$\rho_{DM} \simeq \rho_{DE}$ and $\rho_{DM} \simeq \rho_{CMB}$.

### 2.4.1 "Decoupling" of weakly interacting particles

Particles in the Early Universe are in in thermal equilibrium as long as the rate of particle collisions resulting in energy transfer is high enough to support this equilibrium. Otherwise, if the time interval between subsequent particle interactions is longer than the age of the Universe, particles are "decoupled" (i.e. do not interact).

An example of particles which experienced "decoupling" in the past is given by neutrinos. Neutrinos could be produced and destroyed in weak interaction reactions

$$e^- + e^+ \leftrightarrow \nu_e + \overline{\nu}_e, \qquad e.t.c. \tag{2.4.3}$$

The cross-sections of these reactions are functions of the temperature

$$\sigma_\nu \sim G_F^2 T^2 \tag{2.4.4}$$

(here $G_F = 10^{-5}$ GeV$^{-2}$ is the Fermi constant, which is a quantity of the dimension [mass]$^{-2}$and is numerically close to $G_F \simeq M_W^{-2}$ where $M_W \simeq 100$ GeV is the mass of the W (and Z) bosons transmitting the weak interactions)[1] . To form a quantity of the dimension of cross-section, [cm]$^2$, one has to multiply $G_F^2$ by the square of the energy scale in the problem, which is in our case $T$.

The number density of particles in relativistic gas in thermal equilibrium scales with temperature as

$$n_{e^\pm,\mu^p m,\nu} \sim T^3 \tag{2.4.5}$$

The mean free path of the particles is

$$\lambda_\nu \sim \frac{1}{n\sigma_\nu} \sim \frac{1}{G_F^2 T^5} \tag{2.4.6}$$

Particles in equilibrium should interact at least once during the life time of the Universe. In other words, the mean free path should be shorter than the size of the Hubble radius, $R_H = H^{-1}$ as the moment $t$. To calculate the expansion rate $H$ at the moment $t$ one could use Friedman equation

$$H \simeq \sqrt{G\rho} \simeq \sqrt{GT^4} \tag{2.4.7}$$

Equating $\lambda_\nu$ to $R_H$ one finds

$$\frac{\lambda_\nu}{R_H} \simeq \frac{G^{1/2}T^2}{G_F^2 T^5} \simeq \left[\frac{10^{10}\text{ K}}{T}\right]^3 \simeq 1 \tag{2.4.8}$$

The above equation shows that the neutrino interactions could efficiently maintain neutrinos in thermal equilibrium only at the temperatures higher than $T \sim 10^{10}$ K$\sim 1$ MeV. The Hubble time at this temperature is $t_H = H^1 \simeq 1$ s from the Big Bang. After $t \sim 1$ s. After this moment neutrinos "decouple" from the rest of matter.

One could also notice that as soon as neutrinos decouple, they could not be produced or destroyed anymore, because e.g. the annihilation reaction $\nu + \overline{\nu}$ becomes inefficient. The density of neutrinos changes only in result of expansion of the Universe,

$$n_\nu \sim R^{-3}, \quad T_\nu \sim R^{-1} \tag{2.4.9}$$

In fact, the dilution of the neutrino density with expansion of the Universe always proceeds in the same way as the dilution of other relativistic particles, in particular photons. This means that the density of neutrinos today should be of the same order as the density of

[1] We use Natural system of Units, see Appendix.

photon gas of CMB today. Such neutrinos form a "relic" neutrino gas with temperature comparable to that of the CMB:T

$$T_\nu \simeq 2 \text{ K} \tag{2.4.10}$$

The number density of the neutrino gas is somewhat smaller than the density of CMB:

$$n_{\nu,0} \simeq 10^2 \text{ cm}^{-3} \tag{2.4.11}$$

This means that everywhere around us there is about 100 primordial neutrinos per each cubic santimeter.

If the mass of neutrinos would be $m_\nu \sim 10-100$ eV,the energy density of the primordial neutrinos would be

$$\rho_\nu \simeq 10^{-29} \left[\frac{\sum m_\nu}{100 \text{ eV}}\right] \text{ g/cm}^3 \tag{2.4.12}$$

i.e. of the order of the critical density of the Universe. In this case the primordial neutrinos would constitute the bulk of the Dark Matter. Such dark matter would be nearly undetectable because of extremely low interaction cross-section. It would be not surprising that the Dark Matter discovered via cosmological and astrophysical observations has never been detected before in the laboratory conditions. Massive neutrinos are not considered as viable Dark Matter candidate because there exists an upper limit on neutrino mass, about 1 eV.

**Problem 3.** Weak interactions are also responsible for conversion of protons into neutrons and vise versa: $p + e^- \leftrightarrow n + \nu_e$, $n \to p + e^- + \overline{\nu}_e$.
Estimate how many neutrons per proton are left in the Universe when the temperature drops below $10^{10}$ K, assuming that protons and neutrons are in thermal equilibrium (distributed according to Maxwell distribution) up to the moment when the equilibrium is broken because of the too low rate of the proton-neutron conversion reaction.
Neutron rest energy is higher than that of proton by $m_n - m_p = 1.3$ MeV.

### 2.4.2 Decoupling of heavy particles (Dark Matter)

The neutrinos are light particles, such that at the moment of decoupling their energies were much larger than the rest energy and particles were relativistic. In an opposite case of decoupling of heavy particles, which decouple at the temperature $T < m$, the residual density of the decoupled particles is estimated in a different way. The density of non-relativistic particles of mass $m_{DM}$ in thermal equilibrium is given by the Maxwell-Boltzman distribution

$$n_{DM} = \left(\frac{m_{DM}T}{2\pi}\right)^{3/2} \exp\left(-\frac{m_{DM}}{T}\right) \tag{2.4.13}$$

$m_{DM}$ is the particle mass est la masse du particule. The time between particle interactions is

$$t_{int} = \frac{1}{\sigma_{DM} n_{DM} v_{DM}} \tag{2.4.14}$$

where $\sigma_{DM}$ is the interaction cross-seciton and $v_{DM} \simeq (3T/2m_{DM})^{1/2}$ is the termal velocity. Similarly to the case of neutrinos, we find the moment of decoupling by equating the interaction time to the age of the Universe

$$t_{int} \sim H^{-1} \quad \rightarrow \quad \sigma_{MN} m_{MN} T^2 \exp\left(-\frac{m_{MN}}{T}\right) \sim \sqrt{G} T^2 \tag{2.4.15}$$

This gives the decoupling temperature $T_0$:

$$T_0 \sim -\frac{m_{DM}}{\ln\left[\frac{\sqrt{G}}{\sigma_{DM} m_{DM}}\right]} \tag{2.4.16}$$

Let us assume, for example, that the interaction cross-section is the weak interactions cross-section (2.4.4) $\sigma_{DM} \sim G_F^2 m_{DM}^2$ (the energy scale in the cross section is now $m_{DM}$ rather than $T_0$, since the interacting particles are massive). In this case the argument of the logarithm in the above equation is

$$\frac{\sqrt{G}}{\sigma_{DM} m_{DM}} \simeq 10^{-11} \left[\frac{m_{DM}}{1 \text{ GeV}}\right]^{-3} \tag{2.4.17}$$

so that the logarithm is of the order of 10-100 in a wide range of masses and $T$ is indeed much smaller than $m_{DM}$.

After the moment of decoupling, the total number of particles is conserved. Their density is only diluted by the expansion of the Universe as $R^{-3}$: $n_{DM}(T) \sim n_{DM}(T_0)(T/T_0)^3$. Taking into account that $n_{DM}(T_0)\sigma_{DM} v_{DM} \simeq H(T_0)$, we find

$$n_{DM}(T) = \left(\frac{T}{T_0}\right)^3 \frac{\sqrt{G_N} T_0^2}{\sigma_{DM} v_{DM}} \tag{2.4.18}$$

Taking into account that the decoupling temperature is $T_0 \sim 0.01 m_{DM}$ one could find the present day density of the heavy decoupled relics

$$\rho_{DM} = m_{DM} n_{DM}(T) \simeq \frac{T^3}{0.01 M_{Pl}(\sigma_{DM} v_{DM})} \simeq 10^{-29} \left[\frac{3 \times 10^{-27} \text{cm}^3/\text{s}}{\sigma_{DM} v_{DM}}\right] \text{ g/cm}^3 \tag{2.4.19}$$

by substituting $T_{\simeq}$2.7 K in the above equaiton. Note that the relic energy density does not depend on the particle mass, only on the cross-section.

The thermal velocities of particles at the moment of decoupling are $v_{DM} \sim 0.1c$, so that the interaction cross-section could be estimated as $\sigma_{DM} \sim 10^{-36}$ cm$^2$. The weak interaction cross-section, $\sigma \sim G_F m_{DM}^2$ could be of the order of $10^{-36}$ cm$^2$ for particle masses in the 10-100 GeV range, just at the upper end of the range of masses of particles probed in accelerator experiments. Hypothetical Weakly Interacting Massive Particles (WIMPs) might constitute the bulk of the Dark Matter in the Universe.

Participation in the weak interactions assures that the WIMP DM particles might have been produced in sufficient amounts in the Early Universe, thus providing a possible explanation for the existence of the DM. At the same time, it poses a problem, because the same weak interactions might make these particles unstable. They should cause particle

decays. Indeed, we know from particle physics that e.g. muons decay into lighter electrons via a weak interaction reaction

$$\mu^- \to e^- + \overline{\nu}_e + \nu_\mu \tag{2.4.20}$$

In a similar way, neutron decays into a lighter proton

$$n \to p + e + \overline{\nu}_e \tag{2.4.21}$$

The decay time in both cases could be estimated (up to a numerical factor), based on the dimensional reasons, as

$$t_d \sim \frac{1}{G_F^2 m^5} \tag{2.4.22}$$

where $m$ is the relevant mass scale, $m = m_\mu$ in the case of muon decay and $m \sim m_e$ in the case of neutron decay. In both cases the heavier particle decays into a lighter particle via a reaction which respects the existing conservation laws (like electric charge, baryon and lepton number).

In a similar way, a DM particle is expected to decay on the time scale

$$t_d \sim \frac{1}{G_F^2 m_{DM}^5} \sim 10^{-14} \left[\frac{m_{DM}}{1 \text{ GeV}}\right]^{-5} \text{ s} \tag{2.4.23}$$

This time scale is short enough to rule out the possibility of the WIMP with a mass higher than a fraction of keV. To overcome this problem various WIMP models introduce an additional conserved quantity, which prohibits the decay of WIMP. As an example, one could cite the "R-parity" conservation in the Supersymmetry models of WIMP. The R-parity is a quantum number which is $+1$ for the particles and $-1$ for their supersymmetric partners. Imposing the R-parity conservation makes the lightest supersymmetric particle stable.

Another possibility to prevent the fast decay of the DM particles is to assume that their coupling to normal matter is "extra-weak". An example of this class of models is given by the "sterile neutrino" DM. In this model one introduces one or several new particles which are the right-handed partners of the known left-handed neutrinos. The sterile neutrinos are coupled to ordinary matter only via "mixing" of their wave function with the active neutrinos. The strength of the mixing is characterised by the parameter $\theta^2 \ll 1$ (mixing angle). extra-weakness of the interactions of sterile neutrinos leads to the increase in their decay time

$$t_d \sim \frac{1}{G_F^2 m_{DM}^5 \theta^2} \sim 10^{16} \left[\frac{m_{DM}}{1 \text{ keV}}\right]^{-5} \left[\frac{\theta^2}{10^{-8}}\right]^{-2} \text{ yr} \tag{2.4.24}$$

Choosing small enough $\theta^2$ and low enough mass $m_{DM}$ one could easily find a range of parameter space in which the life time of the DM particle is much longer than the age of the Universe (about $10^{10}$ yr).

However, a particle with "extra-weak" coupling to the normal matter might not be efficiently produced via interactions of conventional matter constituents in the Early Universe. It may even well be that the extra-weakly coupled DM particles never enter the

thermal equilibrium in the Early Universe. In the particular case of sterile neutrinos detailed calculations show that they still might be produced in sufficient amounts via oscillations with the active neutrinos before the moment of active neutrino decoupling.

Sterile neutrino DM model is, along with the WIMPs, a model of the "candidate" DM particle. There is a range of other "candidate" DM particles appearing in different theoretical models of the DM. In each case a viable production mechanism is suggested through which the DM particles were

Different particle physics models of DM could not be distinguished and tested based only on the cosmological considerations. To identify the nature of the DM one has to combine the cosmological considerations with the complementary observational and experimental tools which would verify the DM models in laboratory experiments or with appropriate astronomical data.

# Chapter 3

# Dark Matter

## 3.1 Experimental evidence for the existence of Dark Matter

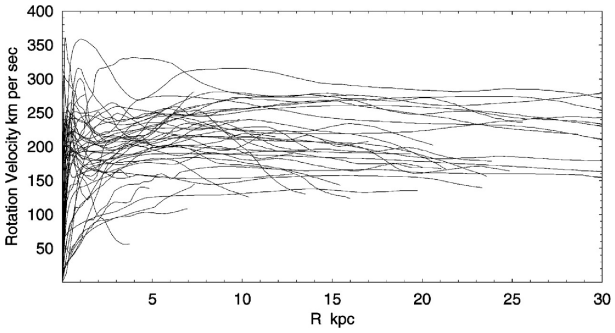


Figure 3.1.1: Rotation curves of spiral galaxies.

Cosmological observations are not the only evidence for the existence of the DM. The term "dark matter" was introduced by Zwicky back in 1930's. Zwicky was interested in dynamics of galaxies inside a galaxy cluster Coma. He found that velocities of the galaxies in the cluster are too high, so that the gravitational field of the cluster, if created by the same galaxies, would not be able to keep the galaxies in the cluster. The finding of Zwicky is somewhat similar to the result which we obtained in the previous chapter for the case of the Universe: if matter visible in telescopes would be the only matter in the Universe, the dynamics of the Universe would be completely different from what is observed.

Today, numerous studies of galaxy clusters confirm Zwicky's result. Detailed studies of the dynamics of spiral and elliptical galaxies show that their mass, similarly to the galaxy clusters, is dominated by the DM.

In the case of spiral galaxies, the main source of information on the galaxy dynamics is the so-called "rotation curve" of the galaxy, which is the velocity of rotation of the galactic disk as a function of the distance form the center. Newton laws suggest that the rotation velocity for a particle (e.g. a star) at the distance $r$ from the galactic center is

$$v = \sqrt{\frac{GM}{r}} \sim r^{-1/2} \tag{3.1.1}$$

where $M(r)$ is the mass contained within the distance $r$ from the center of the galaxy. Outside of the bulk of the mass of the galaxy the rotation velocity should decrease as

$r^{-1/2}$. However, this decrease has (almost) never been observed in any spiral galaxy. Fig. 3.1.1 shows a sample of rotation curves of a large number of spiral galaxies. One can see that in most of the cases the rotation curve is "flat"

$$v \to const \tag{3.1.2}$$

at large distance. This means that the total mass grows as

$$M(r) \sim \frac{v^2 r}{G} \propto r \tag{3.1.3}$$

up to the distances of about 30 kpc from the centres of the galaxies. The total mass inside a radius $r$ is related to the density of matter as

$$M(r) = \int_0^r 4\pi r'^2 \rho(r') dr' \tag{3.1.4}$$

If the mass grows as $M(r) \sim r$ the density decreases as

$$\rho(r) \sim \frac{1}{r^2} \tag{3.1.5}$$

**Problem 4.** Estimate the masses of galaxies $M(r = 10 \text{ kpc})$ for which the rotation curves are shown in Fig. 3.1.1.

If the galaxies would be composed mostly of stars, the matter density would be proportional to the volume brightness, since all star populations have more-or-less fixed mass-luminosity dependence. The surface brighness of a galaxy observed in a telescope is a function of the projected distance from the galactic center $r_0$: $I(r_0) \sim \int_{-\infty}^{\infty} dz \rho(\sqrt{r_0^2 + z^2}) \sim r_0^{-1}$. Observations in the optical band show that the typical surface brightness porfiles of the galaxies have the form

$$I(r_0) \sim \exp(-r_0/r_{core}) \tag{3.1.6}$$

where $r_{core}$ is the size of the galaxy core. An exponential surface brightness profile could be obtained only via integration of an exponentially decreasing function beyond $r_{core}$. This means that the volume mass density of stars decreases exponentially at the peripheries of the galaxies. The mass density of the stars is inconsistent with the volume density of matter derived from the galactic dynamics. This indicates that most of the matter density at the peripheries of galaxies is in the form of DM.

In elliptical galaxies and galaxy clusters we do not observe coherent rotations. Nevertheless, one can measure the mass inside a radius $r$ from the observations of random motions of bodies in these structures. The idea is to use the virial theorem

$$\frac{m \langle v^2 \rangle}{2} \sim \frac{GM(r)m}{2r} \tag{3.1.7}$$

to measure $M(r)$.

In galaxy clusters most of the visible matter is in the form of gas. Random motions of particles in a gas are characterized by temperature $T$, which is about the kinetic energy of random motions:

$$\frac{3}{2}T = \frac{m \langle v^2 \rangle}{2} \tag{3.1.8}$$

Using the virial theorem, we find that the gas temperature at the distance $r$ from the cluster depends on the mass containted within $r$: $T \sim G_N M(r)m/r$. Measurement of the gas temperature as a function of distance form the cluster centre could be used to deduce the mass profile $M(r)$. Typical parameters of galaxy clusters are size $r \sim 1$ Mpc eand mass $M \sim 10^{14} M_\odot$. Typical temperatures are in the X-ray domain

$$T \sim 1 \left[\frac{M}{10^{14} M_\odot}\right] \left[\frac{1 \text{ Mpc}}{r}\right] \text{ keV} \tag{3.1.9}$$

Fig. 3.1.2 shows the X-ray image of Coma cluster (the galaxy cluster studied by Zwicky), obtained with the help of European Space Agency (ESA) X-ray telescope *XMM-Newton*. The diffuse emission visible in the cluster core (red-magenta) and in a sub-cluster on the right bottom part of the image is produced by the hot intracluster gas.

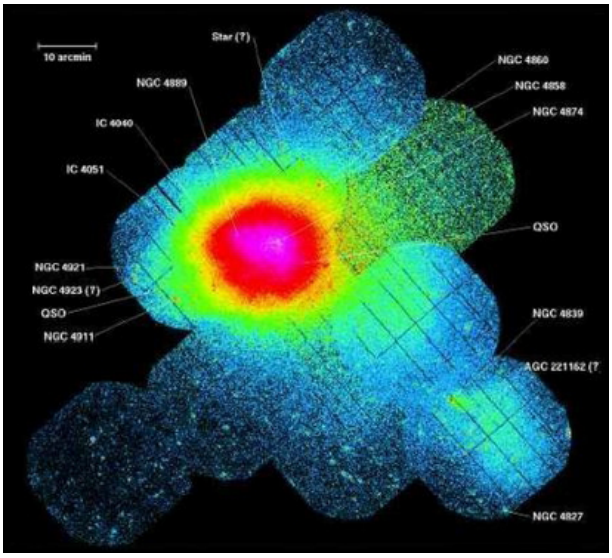


Figure 3.1.2: Image of Coma cluster in the X-ray band.

For most of the galaxy clusters X-ray measurements of the mass profiles give results qualitatively similar to the result found in spiral galaxies: at the periphery of the cluster the mass grows as $M(r) \sim r^\alpha$, $\alpha \sim 1$, with the total mass $M(r)$ normally by a factor of 5-10 larger than the mass of the gas.

## 3.2 Direct detection of DM (for WIMPs).

The rotation curve of our Milky Way galaxy if flat starting from the distance $\sim 1$ kpc form the centre. The Sun is situated at the distance $\simeq 8$ kpc from the Galactic Centre. The rotation velocity is $\sim 200$ km/s. Using Eq. (3.1.1) one can find that the average density of matter within the Solar radius is

$$\rho \simeq 0.2 M_\odot/\text{pc}^3 \tag{3.2.1}$$

The DM contributes a sizeable fraction of this density. The number density in the Solar neighbourhood is

$$n_{DM} \sim 1 \left[\frac{m_{DM}}{1 \text{ GeV}}\right] \text{ cm}^{-3} \tag{3.2.2}$$

where $m_{DM}$ is the mass of the DM particles. If the mass of the DM particles is about 1 GeV, each cubic centimetre in any laboratory should contain a DM particle. One could try to construct an experiment which would be able to catch the DM particles.

The only way to catch the DM particles is to make them interact with the detector medium. The rate of interactions of DM particles in the detector is determined by the DM

– normal matter interaction cross-section which is, of course, not known. An estimate of the cross-section is a part of any theoretical model of the DM. This cross-section could be constrained by cosmological considerations of the DM production in the Early Universe, as it was illustrated in the previous chapter for WIMPs. In the WIMP scenario one assumes that the DM particles interact with the known matter through weak interactions.

The WIMP cross-sections is extremely small, so that WIMP interactions with the normal matter are rare. To detect them on top of background of normal particle interactions, one needs to minimize the rate of interactions of ambient known particles (protons, neutrons, electrons, muons etc) in the detector. To "hide" the detector from the ambient particles, DM detectors are installed in underground laboratories.

One possible way to distinguish the DM signature in the detector from the unrelated background is via characteristic time modulation expected for the DM interactions rate. The Solar system moves around the center of the Milky Way galaxy with the speed $v \sim 200$ km/s. The coherent motion of the Galactic disk is the result of viscous coupling between "normal" matter in the Galaxy. To the contrary, the DM does not participate in the viscous coupling, so that it does not follow the rotation of the disk. Instead, it is distributed in the form of an extended "halo" of randomly moving particles, with velocity dispersion $\langle v_{\rm DM}^2 \rangle \sim v^2 \sim (200 \text{ km/s})^2)$. This means that the velocity of propagation of the Earth though the DM halo is about $\sim 200$ km/s. The speed of rotation of the Earth around the Sun is $\sim 30$ km/s. This rotation velocity changes its direction in the course of the year. This means that the rotation velocity around the Sun could increase or decrease the velocity of motion of the Earth through the DM halo in the range from 170 km/s to 230 km/s. This change of velocity is regularly repeating with a year period.

The flux of DM particles on the detector depends on the velocity of motion the detector through the WIMP halo $v_{rel}$,

$$F_{\rm DM} = n_{\rm DM} v_{rel} \simeq 10^5 \left[\frac{100 \text{ GeV}}{m_{\rm DM}}\right] \left[\frac{v_{\rm DM}}{10^{-3}}\right] \text{ cm}^{-2}\text{s}^{-1} \tag{3.2.3}$$

The annual modulation of $v_{rel}$ is by a factor $(230 \text{ km/s} - 170 \text{ km/s})/230 \text{ km/s} \sim 0.25$, which gives up to 25% variation in the WIMP flux.

The rate of DM interactions in the detector is estimated as

$$R \sim \sigma N_{\rm det} F_{\rm DM} \sim 10^{-7} \left[\frac{\sigma}{10^{-36} \text{ cm}^2}\right] \left[\frac{N}{10^{24}}\right] \left[\frac{100 \text{ GeV}}{m_{\rm DM}}\right] \left[\frac{v_{\rm DM}}{10^{-3}}\right] \text{ s}^{-1} \tag{3.2.4}$$

where $N_{\rm det}$ is the number of "target" particles (atomic nuclei or electrons) in the detector.

The observable effects of WIMP interactions in the detector depend on the energy deposition in each interaction. The main interaction channel for WIMP-normal matter interactions is the elastic collisions with atomic nuclei. If the mass of the DM particles is much larger than the mass of the proton, the atomic nucleus will experience a recoil in collision with a DM particle. The typcial energy of such nuclear recoil could be readily estimated

$$\Delta E_{max} = 2 m_{\rm DM} v_{\rm DM}^2 \sim 1 - 10 \text{ keV} \tag{3.2.5}$$

A small fraction of the recoil energy goes into excitation and/or ionisation of atoms. Rest of the energy goes into excitation of the sound waves in the detector. Detection of the

DM interaction requires, therefore, the detection of keV-scale energy deposition in the detector. This means that the DM detector should, in fact, be an X-ray detector. Indeed, X-ray photons, which typically have energies around keV, also deposit this energy in the detector (e.g. of an X-ray telescope).

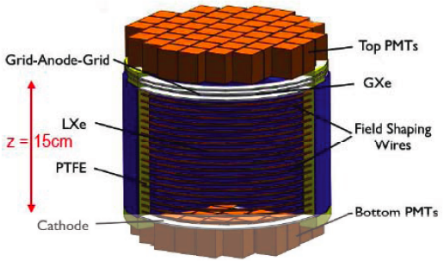


Figure 3.2.1: XENON experiment for DM detection in recoild of atoms in liquid Xenon.

The keV energy deposit in the detector could be detected via one or several measurement techniques:

- detection of ionization produced by DM interactions
- collection of light produced in de-excitation of atoms
- detection of phonons (sound waves) produced by the DM interactions

One possible type of an X-ray detector is CCD ("charge coupled device") used in the digital photo cameras. In CCD, the energy deposit leads to the production of the electron-hole pairs in a semiconductor. Production of one pair rquires about 1 eV energy. a keV energy deposit produces $\sim 10^3$ pairs. The number of pairs produced at each interaction could be measured by applying a potential difference to the semiconductor. The precision of measurement of the energy of the incident X-ray is determined by the statistical fluctuations of the number of pairs.

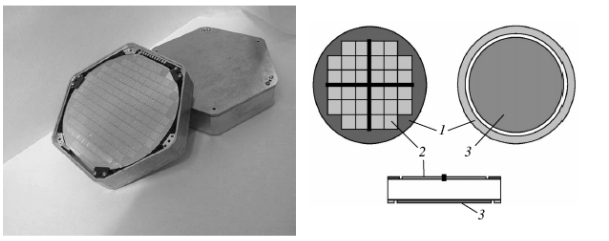


ZIP detectors: (*1*) outer contact (grounded); (*2*) thermistors; and (*3*) inner contact (for readout of the ionization signal).

Figure 3.2.2: CDMS experiment on detection of photons with the help of TES sensors.

Another method for detection of keV energy deposit is to collect scintillation light produced in de-excitation of atoms excited by the DM elastic collisions in materials like NaI or Xe (Fig. 3.2.1). The energy of nucleus recoil is sufficient to create an excited Xe molecule which disintegrates emitting a photon

$$\mathrm{Xe2}^* \rightarrow 2\mathrm{Xe} + \gamma \qquad (3.2.6)$$

Photons produced in the deexcitation of Xe molecules could be detected by photomultipliers looking inside the detection volume (Fig. 3.2.1).

A principally different method is detection of photons (vibrations of the detector) excited in nuclear recoils. One possibility is to measure the increase of temperature of the detector following each DM interaction. The temperature increase is tiny, of the order $T \sim 10$ mK (of course, it depends on the mass and heat capacitance of the detector). To measure such tiny variations of temperature, one uses Transition Edge Sensors (TES). These are suprconductor detectors in which the supervconductor is maintanined at the temperature very close to the critical temperature of superconductor-normal conductor

phase transtion $T_c$. The vibration of the detector produced by the DM interaction leads to the increase of the temperature above $T_c$ and to the increase of the resistivity of the detector which could be measured. The TES sensors are used in the CDMS experiment in US, see Fig. 3.2.2.

The main difficulty of all DM detection experiments is that the nuclear recoils with energy deposition in the keV range could be produced by a variety of processes, even deep underground (e.g. by interactions of particles emitted by the rock). To reduce the rate of background events different techniques are used, such as cooling the detector to very low temperatures, shielding the detector etc. One also tries to distinguish the background signal from real DM recoil events by looking at spectral and temporal characteristics of the signal.

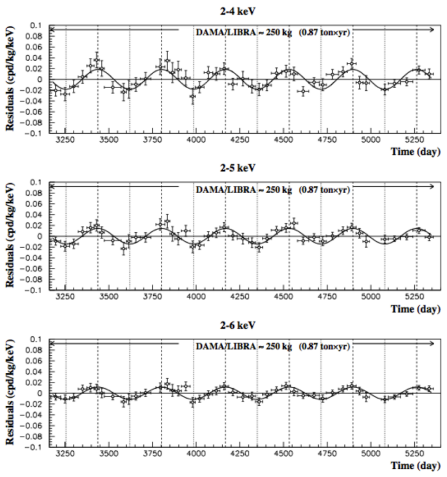


Figure 3.2.3: Annual modulaiton of the signal in DAMA-Libra detector.

Another method of suppression of the background is used by the experiment DAMA-Libra. The idea is to see the annual modulation of the signal caused by the variations of the speed of motion of the Earth through the DM halo. In fact, the annual modulation of the signal is systematically detected by DAMA-Libra, see Fig. 3.2.3. If the annual modulation observed by DAMA-Libra is due to the DM signal, the experimental data provide a measurement of the parameters of the DM particles, the mass and the cross-section, shown in Fig. 3.2.4.

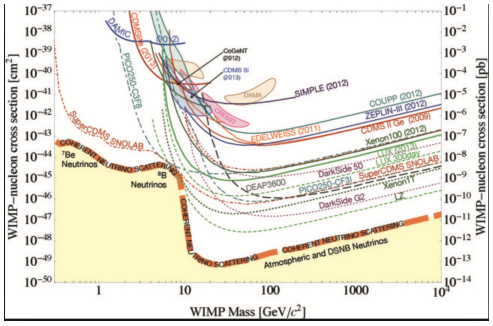


Figure 3.2.4: Experimental limits on WIMP parameters. Claimed "evidences" for the signal by different experiments are shown by different colour coding. The upper limits on the WIMP cross-section from XENON and LUX experiments are shown by green lines. Snesitivities on next-generation detectors are shown by dashed / dotted lines. The level of neutrino background is shown by the yellow shared band.

Other experiments, CRESST (phonons detection method) and CoGENT (ionisation detection in Ge), also detect "excess" events in a way similar to the CDMS, in the regions of parameter space where the DM signal is expected. The claimed significances of the signal are at $2.8\sigma$ (CoGENT) and $4\sigma$ (CRESST) levels. A summary of the estimates of the mass and cross-sections of the DM particles suggested by the experimental results is shown in Fig. 3.2.4.

A number of next-generation direct DM detection experiments is planned, with a planned increase of sensitivity sufficient for verification of the contradictory claims mentionned above. In fact, the sensitivity of the future facilities like DARWIN (next generation liquid Xenon experiment) and DARKSIDE (liquid argon setup) will be sufficient for detection of inevitable neutrino background.

## 3.3 Indirect detection of DM.

The direct detection or production of DM particles in laboratory experiments is possible only in a special case of WIMPs. If we consider the case of "extra-weakly" interacting particles, like the sterile neutrinos with masses in the keV range, we would find that the energy transfer in the reaction of scattering of sterile neutrino on detector particles is in the milli-electronVolt (rather than kilo-electronVolt) range. Besides, the extremely low cross-section of interactions (recall the suppression factor $\theta^2$ in the sterile neutrino cross-section) make the event rate extremely low.

Since we are not sure at all that the WIMP model is the correct model for particle DM, we have to explore alternative possibilities to detect DM particles, to find information complementary to the known effects of gravitational pull of DM observed in the dynamics of galaxies and of the Universe.

Instead of trying to detect the effects of interaction of the DM particles in a laboratory detector, one could try to observe the effects of DM particle interactions in astrophysical conditions. Such an approach has an advantage that the astronomical bodies, which serve as DM detectors in this case, have much larger mass than the laboratory detectors.

The first examples of the massive astronomical bodies are the Earth and the Sun. Simply re-scaling the Eq. (3.2.4) one could find that the rate of DM interactions in the Earth ($M = 6 \times 10^{27}$ g) is some $10^{21}$ s$^{-1}$ for the reference parameters of the cross-section and mass of the DM particle given in the equation. The interaction rate in the Sun is by further 5 orders of magnitude higher ($M_\odot = 2 \times 10^{33}$ g).

An immediate problem for the use of an astronomical body as a DM detector would be to get the DM interaction signal out of the detector. The energy released in the scattering of DM particles in the celestial body would just thermalise inside the body, so that no visible effect of DM interactions would be produced.

A signal from DM interactions which is potentially detectable is when the interaction results in production of photons or neutrinos which could escape from the source and reach a telescope or a neutrino detector on the Earth. Two main possibilities for the processes leading for the potentially detectable (and identifiable over backgrounds) signal are considered: annihilation and decay of DM particles. Both interactions produce energy output $\sim M_{DM}$. in the form of conventional particles, including photons and neutrinos.

**Problem 5.** Assuming that WIMPs interacting with the Sun scatter inelastically with the cross-section $\sigma_{DM-p}$ and remain on bound orbits in / around the Sun after scattering, estimate the number of the DM particles accumulated inside the Sun over its lifetime (5 Gyr). Estimate the flux of neutrinos from WIMP annihilations detectable at Earth. The WIMP annihilatiton cross-section is $\sigma_{DM-DM}$.

The rate of annihilation/decay reactions is highest in the places with the highest concentration of DM. In our Galaxy the place with the highest DM concentration is the region around the Galactic Center. In general, the density of the DM scales with the distance from the Galactic Center, $n_{DM}(r)$. Observation of the rotation curves of the

galaxies suggest $n_{DM}(r) \sim r^{-2}$ in the distance range up to $r \sim 30$ kpc. The behavior of $n_{DM}(r)$ at shorter or larger distances could not be determined directly from the rotation curve (at shorter distances the visible luminous matter contribution should be subtracted, at larger distances the quality of the data is not sufficient). The most common way to estimate the dependence of $n_{DM}$ on $r$ over a wide distance range is to use numerical simulations of formation of the DM halos. One of the most commonly used profiles is the Navarro-Frenk-White profile

$$n_{DM}(r) = \frac{n_0}{(r/r_0)\,(1+(r/r_0)^2)} \tag{3.3.1}$$

Close to the Galactic Center, the DM density is expected to reach very large values, i.e. to have a "spike" $n_{DM}(r) \sim r^{-1}$, if $\alpha \simeq 1$ (typically found in simulations).

The mean free path of the DM particles becomes short in the "spike", $\lambda = (\sigma n)^{-1} \sim r$, the rate of annihilation reaction involving DM particles increases. As a result, stronger signal could be observed from the direction toward the Galactic Center, than from other directions on the sky. Similarly, is the DM particles are occasionally decaying, larger concentration of these particles in the Galactic Center region leads to a higher decay rate.

The interactions of the DM particles in the Galactic halo result in production of the Standard model particles. If the mass of the DM particle is below the electron mass, the only Standard model particles which could be produced are photons and neutrinos. Interactions of the DM with mass in 1-100 MeV range could also result in production of electron-positron pairs. Higher mass DM interactions would also produce muon-antimuon or quark-antiquark pairs etc. Quarks do not exist in free form and they would have to combine into pions $\pi^0, \pi^+$ and $\pi^-$. Photons detectable by telescopes could be either directly produced in DM interactions or they can be secondary particles produced e.g. in the neutral pion decays:

$$\pi^0 \to 2\gamma \tag{3.3.2}$$

Charged pion decays result in production of neutrinos (also potentially detectable on Earth):

$$\pi^\pm \to \mu^\pm + \nu_\mu \qquad \mu^\pm \to e^\pm + \nu_\mu + \nu_e \tag{3.3.3}$$

The energies of particles produced directly in annihilation or decay of the DM particles are close to the rest energy of the DM particles, $E \simeq M_{DM}$. To the contrary, secondary photons from the $\pi^0$ decays A spread of the energies of photons/neutrinos from DM annihilation/decay due to the random motions of the DM particles is very small: $\Delta E/E \sim v_{DM}/c \sim 10^{-3}$, where $v_{DM} \sim 200$ km/s is the typical velocity of DM particles, which is of the order of the rotation velocity of the Galaxy.

The rate of annihilation of the DM particles in the Galactic Center region is proportional to the DM density:

$$\mathcal{R}(r) = \sigma \langle v \rangle (n_{DM})^2 \sim \frac{1}{r^2} \tag{3.3.4}$$

The volume brightness of the DM annihilation signal (number of photons/neutrinos produced per unit time and unit volum) is just $L(r) \sim \mathcal{R}(r)$. An observer looking at the Galactic Center region in a telescope could measure the surface brightness of emission (flux per unit solid angle) as a function of angular distance for the Galactic Center, $\theta$,

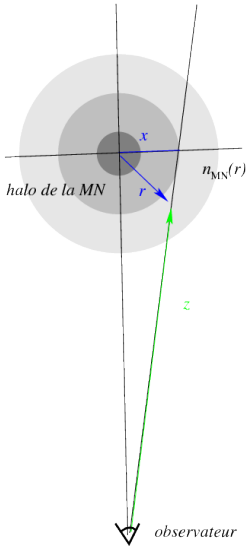


Figure 3.3.1: Geometrical scheme for the calculation of the DM annihilation/decay signal.

or, equivalently, as a function of projected distance on the sky plane, $x = D\theta$, where $D$ is the distance to the Galactic Center (Fig. 3.3). The surface brightness profile could be found via integration of the volume luminosity along the line of sight in each direction $\theta$. Contribution of a layer between $x$ and $x + dx$ is

$$\frac{dL(x)}{dx} \sim 2\pi\rho M_{DM}c^2 \int \mathcal{R}\left(\sqrt{x^2+z^2}\right) dz \tag{3.3.5}$$

so that the flux from the direction $\theta$ is

$$\frac{dF}{d\theta} = \frac{1}{4\pi D^2}\frac{dL(x)}{dx}\frac{dx}{d\theta} = \frac{1}{4\pi D}\frac{dL(x)}{dx} \tag{3.3.6}$$

The overall luminosity of a galaxy due to the DM annihilation could be estimated as an integral of the volume brightness $l = M_{DM}\mathcal{R}(r)$:

$$L = \int 4\pi r^2 dr M_{DM}\mathcal{R} \sim 4\pi M_{DM}\left\langle\sigma v\right\rangle n_0^2 r_0^3 \tag{3.3.7}$$

$$\sim 10^{38}\left[\frac{M_{DM}}{100\text{ GeV}}\right]^{-1}\left[\frac{\langle\sigma v\rangle}{3\times10^{-26}\text{ cm}^2/\text{s}}\right]\left[\frac{r_0}{10\text{ kpc}}\right]\text{ erg/s} \tag{3.3.8}$$

In principle, sources with the luminosity comparable to that estimated above for the reference values of $\sigma$ and $M_{DM}$ are detectable with existing $\gamma$-ray telescopes. However, it turns out that the DM annihilation (decay) is not the only possible source of the $\gamma$-rays from the Galactic Center region. In general the entire Galaxy is a bright $\gamma$-ray source, see Fig. 3.3.2 for an image of the Galaxy in the energy band 0.1-100 GeV, obtained with Fermi space-based $\gamma$-ray telescope. Most of the $\gamma$-ray emission is continuum emission

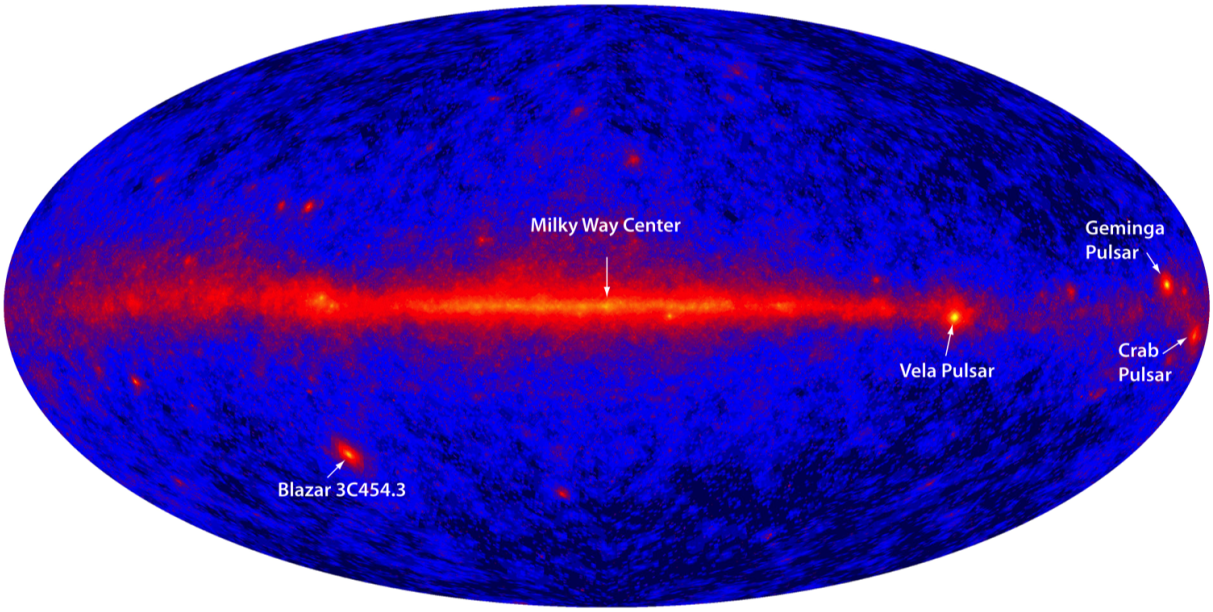


Figure 3.3.2: Emission from the Galaxy in the energy range 0.1-100 GeV detected by Fermi telescope.

produced by interactions of high-energy particles (cosmic rays) ejected from numerous Galactic sources with the interstellar medium matter (Fig. 3.3.2).

**Problem 6.** Consider the case of decaying DM.
Calculate the surface brightness profile of the decay signal on the sky. Estimate the X-ray flux per steradian expected from decaying sterile neutrino DM with mass $M_{DM} \sim 1$ keV with lifetime $\tau \sim 10^{28}$ s.

## 3.4 Indirect detection of DM via secondary particles from annihilation/decay

Decay or annihilation of the DM particles results also in production of charged particles, like electrons and positrons, if the rest energy of the DM particle is sufficiently large for the production of particle pairs. Unstable particles (e.g pions) produced in DM annihilation would decay into stable ones, like electrons/positrons or protons/antiprotons. Secondary charged particles particles from the DM decays could then be detected by the cosmic ray detectors.

The main existing detectors of cosmic rays with energies in the MeV-TeV range are mounted on the high-altitude balloons or installed on the spacecrafts (AMS-02).

In principle, the secondary particles from the DM decay contribute to the fluxes of main cosmic ray species, like protons and electrons. However, similarly to the $\gamma$-ray signal from the DM annihilation, detection of the DM contribution in this case would be difficult, because of the high level of unrelated signal form the cosmic rays themselves. To the contrary, the level of sub-dominant components of the cosmic ray flux, like positrons or antiprotons, is much lower, while the strength of the DM signal in positrons or an-

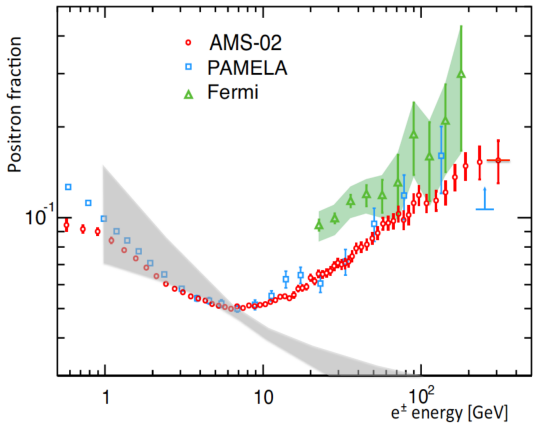


Figure 3.4.1: Spectrum of positrons observed by the AMS-02 experiment. Grey line shows the expected spectrum of secondary positrons from cosmic ray interactions in the Galaxy.

tiprotons is expected to be the same as in electrons or protons. This means that the DM signal could be found at the first place as a feature in the spectra of these sub-dominant components. Positrons and antiprotons are also produced in interactions of cosmic rays with the interstellar material or in the cosmic ray sources. However, the spectral shape of the secondary positrons or antiprotons from the cosmic ray interactions is powerlaw. This shape is very different from a narrow spectral features concentrated toward the rest energy of the DM particles, expected from the DM signal. This difference in the spectral shape facilitates the search of the DM contribution in the cosmic ray data.

A strong feature in the spectrum of the positron component was recently reported by AMS-02 detector (Fig. 3.4.1 at the energies above 10 GeV. The origin of this feature is not clear for the moment. One of the possible explanations involves the secondary particles form the DM annihilation. Annihilation of the DM particles into electrons and positrons is expected to result in the production of continuum spectrum of positrons with energies somewhat below the DM rest energy. This should produce a "bump" in the positron spectrum. The "DM bump" is an addition to the spectrum of positrons produced in a conventional way in the interactions of high-energy cosmic rays in the Galaxy.

The DM bump is not the only possible explanation of the "positron excess". AN alternative possibility is that positrons of the energies 10-100 GeV are directly produced in nearby astronomical sources and then propagate through the interstellar medium up to the Earth.

## 3.5 DM production in collider experiments.

A different approach to the search of the WIMP dark matter is the attempt to search for the production of DM particles in high-energy collisions at LHC. If the venter-of-mass energy of particle collisions is higher than twice the DM particle mass, collisions of known high-energy particles could occasionally result in production of DM particle-antiparticle pairs. In the absence of special cancellations in the scattering amplitude, the reaction of the DM production in particle collisions is expected to have approximately the same

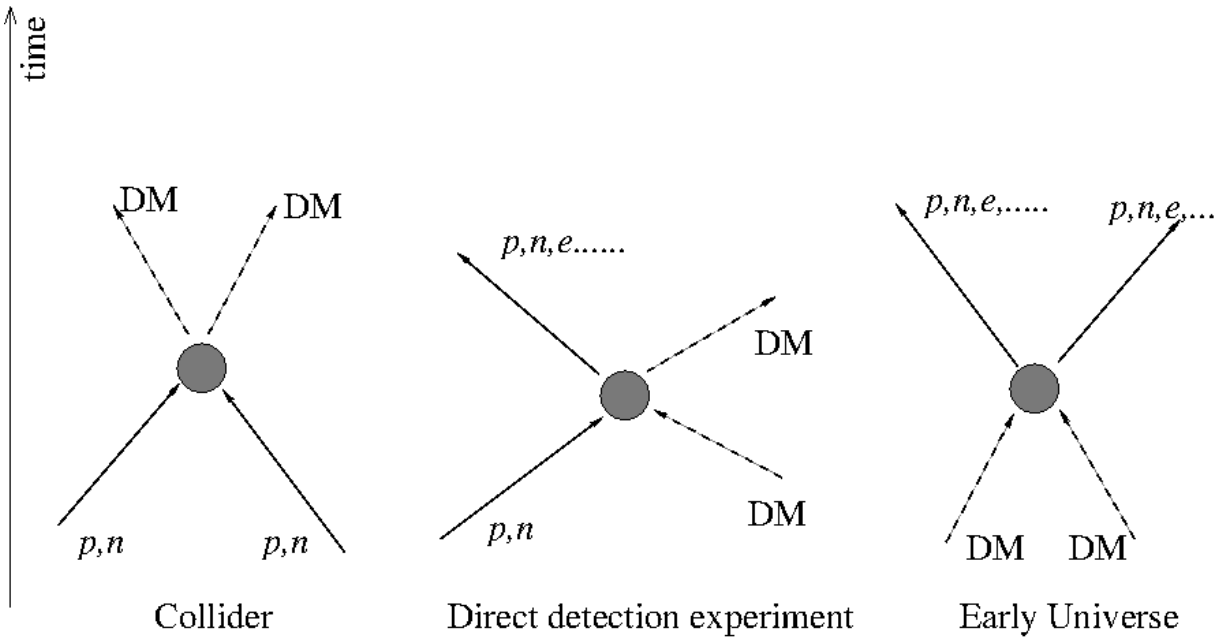


Figure 3.5.1: Different interaction channels of DM.

cross-section as the reaction of DM – normal particle collisions and the reaction of the DM annihilation in the Early Universe (see Fig. 3.5). In the WIMP model, the cross-section of these reactions is always estimated as $\sigma \sim \kappa G_F^2 E_1 E_2$ for the energy scales of colliding particles lower than the W boson mass and $\sigma \sim \kappa\alpha / E_1 E_2$ for the collisions at the energies higher than the W boson mass. Measuring the cross-section in one type of reaction one could estimate the cross-section of reaction involving DM particles in different channels.

A comparison of the limits on the DM interaction cross-section derived from non-observation of DM-producing reactions at LHC experiments and the limits on the cross-section from the direct detection experiments is shown in Fig. 3.5.

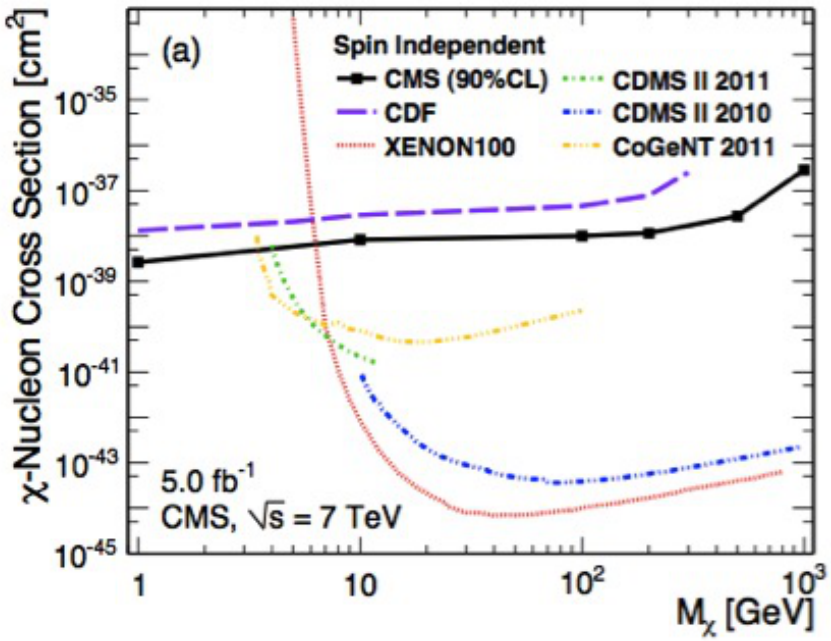


Figure 3.5.2: Limits on the WIMP DM interaction cross-section from LHC experiments.

# Chapter 4

# High-energy processes in stars

## 4.1 Evolution of massive stars

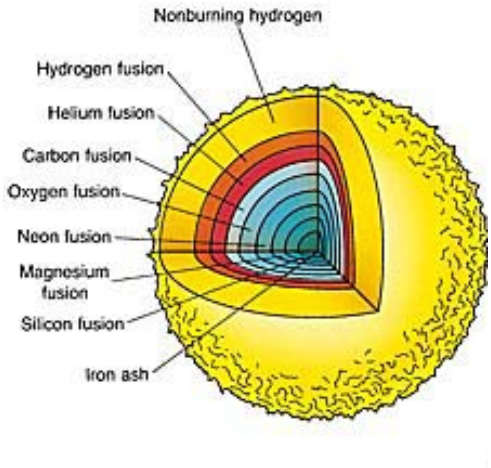


Figure 4.1.1: Internal structure of a massive star at the end of evolution before the supernova explosion.

Stellar evolution proceeds through the synthesis of heavier elements, from the lighter ones (starting from the primordial H, He). At the end of each stage of evolution (e.g. synthesis of He from H) the energy output of nuclear reaction diminishes. This leads to the decrease of the radiation pressure and to contraction of the part of the star not supported by the radiation anymore. Contraction reheats the star and starts next stage of nuclear synthesis. The process could repeat up to the point at which Fe nuclei are produced in nucleosynthesis. At the end of evolution, the star is composed of several layers of different elements, like it is schematically shown in Fig. 4.1.1.

The "nucleus" of the evolved star which is composed of iron, the nuclear reactions stop because the synthesis of still heavier elements is not possible energetically (the nuclear binding energy of heaver elements is smaller than that of iron).

The iron core is in hydrostatic equilibrium with pressure $P$ at distance $r$ balancing the gravity force on a unit volume element with density $\rho$:

$$\frac{dP}{dr} = \frac{GM\rho}{r^2} \tag{4.1.1}$$

The main contribution to the pressure is that of degenerate electron gas. Electrons are fermions and the relation between the pressure and density of electron gas could be derived directly from the Heisenberg uncertainty relation $\Delta p \Delta x \sim 1$ in the following way. The mean distance between particles in the gas of density $n$ is $\Delta x \simeq n^{-1/3}$. The momentum of non-relativistic particles is $\Delta p = mv$ where $m$ is the particle mass and $v$ is its velocity.

Assuming $\Delta p \sim p \sim (\Delta x)^{-1} \sim n^{1/3}$ one finds that the pressure of a gas of non-relativistic fermions is

$$P \sim nvp \sim \frac{n_e^{5/3}}{m_e} \tag{4.1.2}$$

Averaging the hydrostatic equilibrium equation over the volume of the iron core or the size $R$ one finds

$$\begin{aligned} \frac{P}{R} &\sim \frac{GM^2}{R^5} \\ \frac{Y_e^{5/3} M^{5/3}}{m_p^{5/3} m_e R^6} &\sim \frac{GM^2}{R^5} \\ R &\sim \frac{Y_e^{5/3}}{G m_p^{5/3} m_e M^{1/3}} \end{aligned} \tag{4.1.3}$$

where $Y_e$ is the ratio of the number of electrons to the number of nucleons, so that $n_e \sim Y_e M/(m_p R^3)$.

The last equation tells that accumulation of the iron "nuclear waste" in the stellar core which leads to the growth of the core mass $M$ also leads to the decrease of the core size $R$. The contraction, in turn, leads to the increase of the density of degenerate electron gas. The increase of the density of electron gas leads to the increase of velocities of electrons, $v \sim n^{1/3}/m_e$.

At some point of the stellar evolution, typical velocities of electrons in the stellar core become comparable to the speed of light. At this moment the equation of state of degenerate electron gas changes from non-relativistic, $P \sim n^{5/3}$ to the relativistic one, $P \sim n^{4/3}$ (if one changes $v \simeq c$ in Eq. (4.1.2)).

An immediate consequence of the change of equation of state is modification of the conditions of hydrostatic equilibrium to

$$\frac{P}{R} \sim \frac{Y_e^{4/3} M_*^{4/3}}{m_p^{4/3} R^5} \sim \frac{G_N M_*^2}{R^5} \tag{4.1.4}$$

which has the only solution

$$M_{Ch} \sim \frac{Y_e^2 M_{Pl}^3}{m_p^2} \simeq 1.4 M_\odot \tag{4.1.5}$$

This fundamental mass scale is named Chandrasekhar mass.

As soon as the stellar core reaches the mass $M_{Ch}$, any further accumulation of the "nuclear waste" in the core would lead to an instability, since the hydrostatic equilibrium equation does not have solutions with $M$ exceeding $M_{Ch}$. At this moment the only possible further step of the stellar evolution is the gravitational collapse of the core.

### 4.1.1 Gravitational collapse

Evolution of the stellar core during the gravitational collapse is, in a sense an inverse of the evolution of the Early Universe which was considered in the previous chapters.

Increase of the density of matter leads to the heating of the medium, which is opposite to the cooling accompanying the expansion of the Universe.

The size of the stellar core just before the onset of collapse is

$$R_{\rm Ch} \sim \frac{Y_e^{5/3}}{G m_p^{5/3} m_e M_{Ch}^{1/3}} = \frac{Y_e^{5/3} M_{Pl}}{m_e m_p} \simeq 10^9 \text{ cm} \tag{4.1.6}$$

about the size of the Earth. Matter density at the onset of the gravitational collapse is

$$\rho_{\rm Ch} = \frac{3M_{\rm Ch}}{4\pi R_{\rm Ch}^3} \sim 10^7 \text{ g/cm}^3 \tag{4.1.7}$$

This density is much higher than the density of matter which one could find in conventional laboratory conditions (compare with e.g. the density of water $\sim 1$ g/cm$^3$). At the same time, this density is much lower than the density in the interior of atomic nuclei. It is also much lower than the characteristic density which one could ascribe to protons or neutrons. Dividing the proton mass by the cube of its radius $r_p \sim 10^{-13}$ cm one finds

$$\rho_N \sim \frac{m_p}{r_p^3} \simeq 10^{15} \text{ g/cm}^3 \tag{4.1.8}$$

Contraction of matter distribution in the process of gravitational collapse should lead to increase of the density, perhaps up to the atomic nuclei density scales.

An obstacle to a prompt gravitational collapse of an unstable configuration is heating of the collapsing matter by the released gravitational energy. Applying the virial theorem to the collapsing core one finds that the temperature should reach some

$$T \sim \left\langle \frac{m_p v^2}{2} \right\rangle \sim \frac{GMm_p}{2R} \sim 25 \left[\frac{R}{10^6 \text{ cm}}\right]^{-1} \left[\frac{M}{M_\odot}\right] \text{ MeV} \tag{4.1.9}$$

as soon as the entire core shrinks to the size of about 10 km.

This temperature is higher than the difference of mass between proton and neutron $m_p - m_n \simeq 1.3$ MeV and than the typical binding energies of atomic nuclei. This has two consequences. First, occasional collisions of atomic nuclei in the collapsing core result in their breakdown, so that the process of graviational collapse "undoes" all the nucleosynthesis work done at the previous stages of stellar evolution. Next, collisions between free protons and neutrons in the collapsing matter could convert protons into neutrons and vise versa.

Neutrons could be produced via the "electron capture" reaction

$$p + e^- \to n + \nu_e \tag{4.1.10}$$

The electron participating in this reaction is taken from the Fermi "sea" and has the energy close to Fermi energy which, for the marginally unstable configuration is about the rest energy of electron. The neutrino produced in electron capture freely escapes from the core and takes away energy. The collapsing core of a massive star should, therefore, be a strong source of neutrinos (see below).

At the same time, the neutron decay reaction

$$n \to p + e^+ + \overline{\nu}_e \tag{4.1.11}$$

could not proceed in the same way as it does in the low density environment, because the electron which should be produced in this reaction has to return to the degenerate Fermi gas, in which all the states up to the Fermi energy $E_F \simeq m_e c^2$ are already occupied. In this way, the neutron decay is suppressed and the entire matter of the core gets gradually saturated with the neutrons which could not decay, the process called neutronization.

Nuclear reactions, in particular, massive production of neutrons, transform the state of matter in the collapsing body. It is possible that at some stage of this transformation the equation of state of matter will change in such a way that the pressure of matter would again support the configuration from further collapse.

This indeed happens at the moment when the pressure of degenerate Fermi gas of neutrons, rather than electrons, becomes important. A relation between the mass $M_{NS}$ and size $R_{NS}$ of the new stable configuration could be found from the equation of hydrostatic equilibrium in a way similar to the one used before to find the mass and size of the stellar core.

## 4.2 Proto-neutron star and neutrino emission

The collapse resulting in formation of the neutron star proceeds on the free-fall time scale

$$t_{ff} \sim \frac{R_{Ch}}{v_{ff}} \simeq \frac{R_{Ch}}{\sqrt{GM_{Ch}/R_{Ch}}} \sim \frac{M_{Pl}}{m_e^{3/2} m_p^{1/2}} \simeq 0.1 \text{ s} \tag{4.2.1}$$

The collapse stops when the configuration supported by the pressure of degenerate neutron gas. The size of this configuration could be estimated by replacing $m_e$ with $m_p$ in expression for $R_{Ch}$. This gives $R_{NS} \sim 10^6$ cm. The gravitational energy released in the collapse is

$$E_{grav} = \frac{G_N M_{Ch}^2}{R_{NS}} \sim 10^{53} \text{ erg} \tag{4.2.2}$$

This energy could be released only through neutrino emission. Typical energies of these neutrinos are about the kinetic energies of particles in the collapsing body, which could be esstimated from the virial theorem,

$$T_{\rm NS} \sim \left\langle \frac{m_p v^2}{2} \right\rangle \sim \frac{GM_* m_p}{2R} \sim 25 \text{ MeV} \tag{4.2.3}$$

The density of the newly formed stable configuration is

$$\rho_{\rm NS} \sim \frac{M_{NS}}{R_{NS}^3} \sim 10^{14} \text{ g/cm}^3 \tag{4.2.4}$$

is of the order of density of an atomic nucleus. The density is, in fact so high that neutrinos are the only particles able to escape from the collapsed body and to cool the body by carrying away energy.

The mean free path of neutrinos is estimated as $\lambda_\nu = (\sigma_W \rho_{NS}/m_p)^{-1}$ where the cross-section of weak interactions is

$$\sigma_{\rm weak} \sim G_F^2 T_{NS}^2 \simeq 10^{-41} \left[\frac{T}{25\ {\rm MeV}}\right]^2\ {\rm cm}^2 \tag{4.2.5}$$

Numerically,

$$\lambda_\nu = \frac{m_p}{\sigma_{\rm weak}\rho_{NS}} \simeq 10^3 \left[\frac{\rho_{\rm NS}}{10^{14}\ {\rm g/cm}^3}\right]^{-1}\ {\rm cm} \tag{4.2.6}$$

The mean free path of neutrinos is shorter than the size of the neutron star so that neutrinos could not escape from deep interior of the neutron star. In this region they participate in the nuclear reactions, like they did in the Early Universe before the moment of neutrino decoupling. They could escape only from a surface called "neutrinosphere" (by analogy with the "photosphere" of conventional stars) at which the depth to the surface of the star is equal to the mean free path. Inside the neutrinosphere the neutrinos are trapped.

Inside the neutrinosphere propagation of neutrinos could be considered as random walk with mean free path $\lambda_\nu$. The time needed for a neutrino produced deep inside the star to reach the surface of the neutron star could be estimated as

$$t_\nu \sim \frac{R_{NS}^2}{\lambda_\nu} \sim 1\ {\rm s} \tag{4.2.7}$$

This is the characteristic time scale of cooling of the proto-neutron star by the neutrino emission.

The cross section of electromagnetic interactions is many orders of magnitude larger than the cross-section of weak interactions, $\sigma_{\rm em} \sim \sigma_T \simeq 10^{16}\sigma_{\rm weak}$ . The diffusion time of photons toward the surface of the neutron star is, therefore, many orders of magnitude larger than the diffusion time of neutrinos. Cooling of the proto-neutron star by the photon emission is not possible.

### 4.2.1 Neutrinos from SN 1987A

The pricture of the end stage of evolution of a massive star described above could be tested via detection of neutrino emission which is associated to the process of neutronization during the core collapse leading to formation of the proto-neutron star and to the process of cooling of the proto-neutron star.

The rate of the core collapse events of massive stars in our Galaxy is roughly 1 per 100 yr. This means that nearby Galactic core collapse events which might provide the strongest neutrino signal are rare. Different types of neutrino detectors with sensitivity sufficient for detection of neutrino flux from Galactic core collapse events exist only since some $\sim 30 - 40$ yr.

The only convincing case of detection of neutrino emission from an astronomical source other than the Sun was the detection of neutrinos from a core-collapse supernova SN 1987A which was situated in a sattelite galaxy of the Milky Way, called Large Magellanic Cloud (LMC).

The distance to the LMC is $D_{LMC} \simeq 50$ kpc. Estimate the typical neutrino flluence from the process of proto-neutron star cooling gives the neutrino flux

$$F_\nu \sim \frac{0.1 E_{grav}}{4\pi D_{LMC}^2} \sim 3 \times 10^4 \frac{\text{erg}}{\text{cm}^2} \tag{4.2.8}$$

so that the total number of neutrinos which passed through each square centimeter was about

$$N_\nu \sim \frac{F_\nu}{E_\nu} \sim 10^9 \text{ cm}^{-2} \tag{4.2.9}$$

At the time of SN 1987A event the existing neutirno detectors had physical size of the order of $R_{det} \sim 10$ m, so that the total number of neutrinos which passed through the detectors was about $N_\nu R_{det}^2 \sim 10^{15}$. The cross-section of neutrino interactions with matter is extremely small, so that only a small fraction of these huge neutrino number could have interacted inside the detectors. Typical density of the detector matter is $\rho_{det} \sim 1$ g/cm$^3$. The mean free path of neutrinos through the detector matter is $\lambda = (\sigma_W \rho_{det}/m_p)^{-1} \sim 10^{16}$ cm, assuming the cross-section of weak interactions $\sigma \sim 10^{-40}$ cm$^2$ in the relevant energy range $E_\nu \sim 10 - 100$ MeV. This means that the probability for a neutrino to interact inside the detector was $p \sim R_{det}/\lambda \sim 10^{-13}$. Thus, out of $\sim 10^{15}$ neutrinos passing through the detector only about $\sim 10^2$ have interacted there. Assuming that the efficiency of detector is some 10% (i.e. only a fraction of the neutrino interaction events in the detector would be noticed) one finds that the 10 m size neutrino detectors could have found some ten(s) of neutrinos coming from a core collapse event in the LMC.

The neutrino signal from SN 1987A was detected simultaneously (all detections within $\sim 10$ s time window) be several neutrino detectors, Kamiokande in Japan, IMB in In US and Baksan in Soviet Union. All in all these three detectors found some 25 neutrinos with energies in the range 10-40 MeV. The arrival times of these neutrinos and their energies are shown in Fig. 4.2.1.

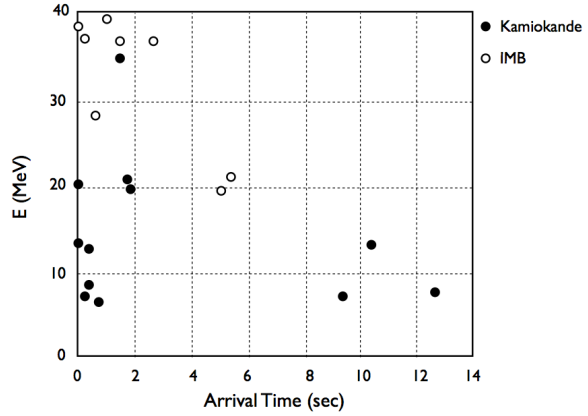


Figure 4.2.1: Neutrino signal from SN 1987A.

Detection of the neutrino flux from a known core collapse event, with the time, energy and overall fluence consistent with the theoretical expectations provides a strong support for the core collapse scenario described above.

The techniques of neutrino detection have significantly evolved sing the SN 1987A event. With the next supernova explosion in our Galaxy or in a Milky Way satellite galaxy, detailed time and energy evolution of the neutrino signal will be studied, because the expected statistics of the neutrino events will be orders of magnitude higher than in the SN 1987A event.

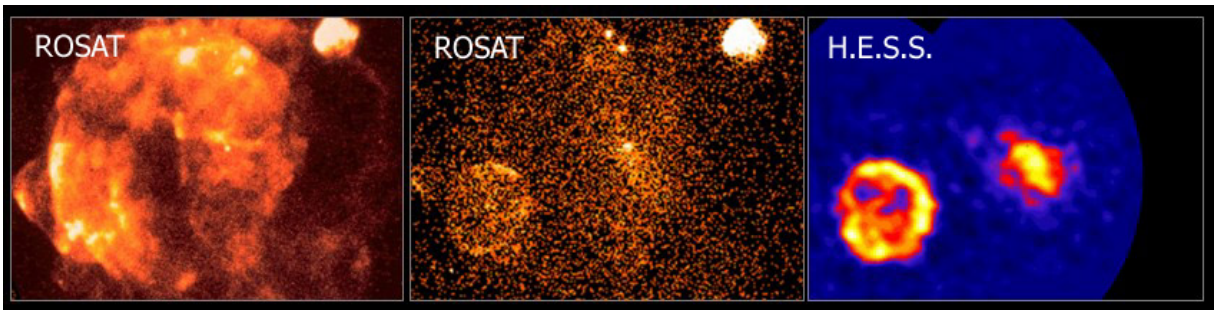


Figure 4.2.2: X-ray and TeV gamma-ray images of a region of sky containing Vela (larger bubble, 5 degrees diameter), Vela Junior (smaller bubble on the left) and Puppis A (bubble on the right top) supernova remnants.

### 4.2.2 Supernova and supernova remnants

Following the gravitational collapse, a significant fraction of massive stars produces supernova explosions in which an outer part of the stellar envelope is ejected carrying overall kinetic energy

$$E_{SN} \sim 10^{51} \text{ erg} \sim 10^{-2} E_\nu \tag{4.2.10}$$

which constitutes only a small fraction of the energy carried away by neutrinos. This kinetic energy is estimated from the observations of expanding supernova remnant shells like those shown in Fig. 4.2.2. In this figure one could see three shells superimposed on each other, with the biggest one being the shell around Vela supernova remnant, which is visible in the "soft" band simage of ROSAT X-ray telescope (left), Smaller shell is "Vela Junior" supernova remnant visible in the hard band of ROSAT (middle) and also in the TeV energy band (right). Still smaller shell is that of Puppis A supernova. The expansion velocity of the supernova ejecta reaches $V_{ej} \sim 10^9$ cm/s, for the ejecta mass $M_{ej} \sim M_\odot$, which provides an estimate $E_{SN} = M_{ej} V_{ej}^2/2 \sim 10^{51}$ erg.

The details of the mechanism of ejection of the matter from the envelope are not clear. The most popular idea is that of "neutrino driven supernova explosion". In this scenario the ejection of a part of the stellar envelope happens because of the excess pressure produced by neutrinos escaping from the neutron star. Indeed, the energy flux of neutrinos traversing the stellar envelope is so high that a small fraction of this energy flux absorbed in the envelope would already deposit sufficient energy to eject the envelope matter. However, the simplest versions of "neutrino-driven supernova explosion" scenario do not work and it is perhaps a combination of neutrino pressure plus the large scale 3d motions of matter in the collapsing star (different hydrodynamical instabilities) which produce the explosions.

### 4.2.3 Neutron stars

Neutron stars, formed in result of gravitational collapse of massive stars, are one of the main source classes in high-energy astrophysics. They are probably observed as X-ray emitting "compact central objects" inside the remnants of supernova explosions. Isolated

neutron stars power activity of radio / gamma-ray pulsars. They are also responsible for the observed X-ray emission from a large fraction of X-ray binaries. Before moving into the discussion of observed astrophysical phenomena produced by the neutron stars, we review in this section the existing understanding of the physical properties of these objects.

Basic estimates of the properties of neutron stars derived from the consideration of the gravitational collapse already give order-of-magnitude estimates for the mass, size and density of these objects, in the range $M_{NS} \gtrsim 1.5 M_\odot$, $R_{NS} \sim 10$ km, $\rho_{NS} \sim 10^{15}$ g/cm$^3$. Several more parameters which were not discussed in the previous section are the spin and magnetic field. First "naive" estimates of these parameters at the moment of the birth of the neutron star could be obtained from the laws of conservation of angular momentum and magnetic flux

$$\begin{aligned} L &= MR^2/P \sim const \\ \Phi &= BR^2 \sim const \end{aligned} \tag{4.2.11}$$

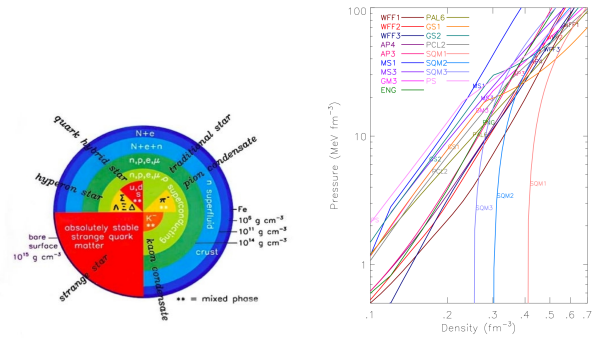


Figure 4.2.3: Different theoretical models of the structure of neutron stars (left) and calculations of equation of state of nuclear matter inside the neutron star (arXiv:1305.3510).

where $P$ is the rotation period, $B$ is the magnetic field. Taking the Sun as the (best studied) example of a non-collapsed star, we use the estimates $B_\odot \sim 1-100$ G, $R_\odot \sim 10^{11}$ cm for the magnetic field and size and get

$$B_{NS} \sim B_\odot \frac{R_\odot^2}{R_{NS}^2} \sim 10^{12} \text{ G} \tag{4.2.12}$$

as an estimate of the magnetic field. Rescaling of the rotation period $P_\odot 2 \times 10^6$ s (26 days) gives

$$P_{NS} \sim P_\odot \frac{R_\odot^2}{R_{NS}^2} \sim 10^{-4} \text{ s, (?)} \tag{4.2.13}$$

for the initial spin period of the neutron star. This spin period is extremely short. It is comparable or shorter than the minimal possible period determined by the conditions of "rotational breakdown" of a star (rotation velocity is equal to Keplerian velocity):

$$v_{rot} = \frac{2\pi R_{NS}}{P_{NS}} \lesssim \sqrt{\frac{G_N M_{NS}}{R_{NS}}} = v_K, \tag{4.2.14}$$

which gives

$$P_{NS} \gtrsim 2\pi \sqrt{\frac{R_{NS}^3}{G_N M}} \simeq 5 \times 10^{-4} \text{ s} \tag{4.2.15}$$

Thus, the collapsing star possibly needs to get rid of angular momentum in the collapse process before the formation of the neutron star. The mechanisms of removal of the

angular momentum being not completely understood, the initial spin periods of the neutron stars at birth are uncertain. However, it is natural to expect that they are in the millisecond range.

Small size of the neutron star leads to an extremely strong gravitational field at its surface. The strength of the gravitational potential is

$$U_{grav} = \frac{G_N M_{NS}}{R_{NS}} \simeq 0.2 \tag{4.2.16}$$

compared to some $10^{-5}$ at the surface of the conventional stars. This means that the space-time near the neutron star is significantly curved and the description of physical processes in and around the neutron star should be based on relativistic gravity considerations.

Similarly to the conventional stars, the hydrostatic equilibrium of the neutron stars is supported by the balance between the gravity force and matter pressure. The matter pressure is provided by the degenerate gas of neutrons, with additions from the pressure of other matter forms present in the star (protons, atomic nuclei).

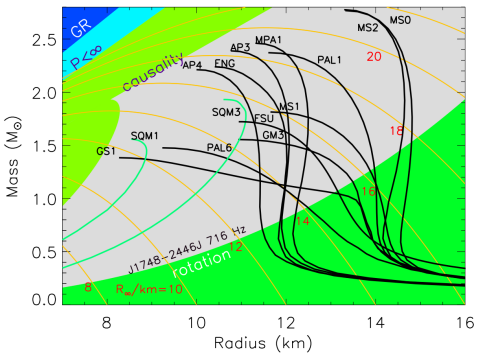


Figure 4.2.4: Theoretically expected mass-radius relations in different models of neutron star equation of state.

The equation of state of the nuclear matter inside the neutron star has contributions from both the degeneracy pressure of the Fermion gas and from the interactions of particles via the strong forces. This leads to a change of the scaling of the pressre with density of the form

$$P \sim \rho^{\gamma} \tag{4.2.17}$$

with the exponent closer to $\gamma \simeq 2$ (Fig. 4.2.3) rather than $\gamma = 5/3$ as for the non-relativistic Fermi gas. This leads to the mass-radius relation of the form

$$R_{NS} \sim M_{NS}^{\frac{\gamma-2}{3\gamma-4}} \sim M_{NS}^{0} \tag{4.2.18}$$

that is $R_{NS}$ is expected to be roughly independent of the mass in some mass range. This is indeed what is predicted by a set of models shown in Fig. 4.2.4. Theoretical models with the predict that the neutron stars should exist only in a narrow mass range, $1.4M_{\odot} \lesssim M_{NS} \lesssim 3M_{\odot}$. The lower bound is determined from the mechanism of formation of neutron stars and the upper bound is given by the limits of relativistic hydrostatic equilibrium conditions.

Measurements of masses and sizes of the neutron stars are potentially important in the general context of Fundamental Physics, because they would provide tests of the theoretical model calculations involving strong gravity theory (presumably General Relativity) and the theory of strong interactions. The physical conditions under which the tests of these theories would be achieved are impossible to create in laboratory conditions here on Earth.

Measurements of masses of neutron stars are most conveniently done via observations of dynamics of these objects which are parts of binary systems. The set of neutron star masses estimated in this way is shown in Fig. 4.2.5. Measurements of the radii of the neutron stars are possible through the measurement of their temperatures $T_{NS}$ and luminosities $L$. This allows to derive the size $R_{NS} \sim L/T_{NS}^4$. Observations of thermal X-ray emission from neutron stars are challenging because of the low brightness of the sources and contamination from other X-ray emission processes (e.g. generated by the accretion onto neutron star surface).

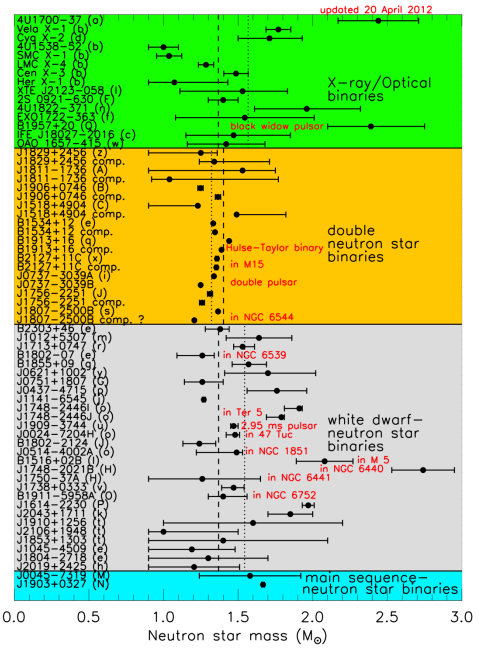


Figure 4.2.5: Measurements of masses of the neutron stars.

## 4.3 Pulsars and pulsar wind nebulae

Young neutron stars reveal themselves in a spectacular phenomenon of pulsars. Pulsars are astronomical sources of highly regular pulsed emission with periods in the range between 1 ms and $\sim 10$ s powered by fast-rotating magnetised neutron stars. The most famous example of pulsar and pulsar wind nebulae is the Crab Nebula shown in Fig. 4.3.1. The center of the nebula hosts Crab pulsar which has the period $P = 33$ ms. Its spin-down power is $\dot{E}_{\rm rot} \sim 10^{38}$ erg/s. The system is situated at the distance $d \simeq 2$ kpc. It is a remnant of a supernova explosion which was observed by Chinese astronomers in AD 1054, so the system is just about $10^3$ yr old.

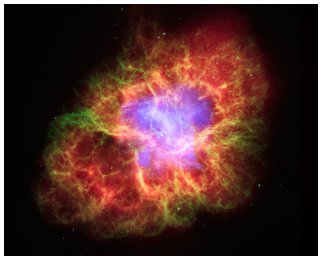

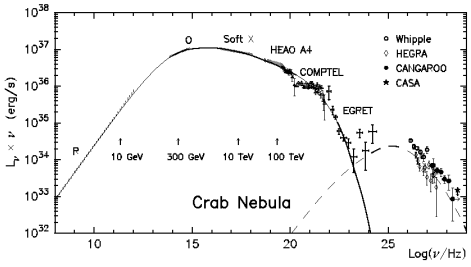


Figure 4.3.1: Multi-wavelength image (left) and broad band spectrum (right) of the Crab nebula.

Different colors in Fig. 4.3.1 show images in different wavebands: blue is the X-ray image, green is in visible and red is in radio. The broadband spectral energy distribution of the source (the power emitted as a function of the photon energy) is shown in Fig. 4.3.1. The luminosity reaches maximum of $10^{37}$ erg/s per decade of energy in the visible-to-X-ray. Integrating the luminosity over the spectrum one finds that close to 100% of the spin-down power of the pulsar is converted into the power of electromagnetic radiation from the nebula. The conversion mechanism

should inevitably involve particle acceleration. Indeed, photons with energies up to 10-100 TeV have to be produced by charged particles (electrons) accelerated to energies much higher than their rest energy.

The experience of operation of particle accelerators on Earth shows that the process of particle acceleration is always accompanied by synchrotron radiation which finally limit the maximal attainable particle energies. The energy of synchrotron photons is

$$E_{\rm synch} \sim \frac{eBE^2}{m^4} \simeq 5 \left(\frac{m_e}{m}\right)^4 \left[\frac{B}{10^{-4}\ {\rm G}}\right] \left[\frac{E}{10^{15}\ {\rm eV}}\right]^2 \ {\rm MeV} \qquad (4.3.1)$$

where $E$ is the energy of emitting particle, $e$ is its electric charge, $m$ is the particle mass and $B$ is the magnetic field strength (in terms of Fig. 4.3.1, photon energy 1 MeV corresponds to the frequency $\nu = E/(2\pi\hbar) = 2.4 \times 10^{20}$ Hz, approximately the energy at which the power output from the source starts to decrease). The broad "bump" extending from radio to 100 MeV gamma-ray band in the spectrum of Crab nebula (Fig. 4.3.1) is conventionally attributed to the synchrotron radiation.

If the magnetic field in the nebula is known, Eq. 4.3.1 gives an estimate of the energy of electrons emitting in the 100 MeV band. An estimate of the magnetic field could be made if one interprets the high-energy bump of Crab nebula spectrum (at 100 GeV energy, Fig. 4.3.1) as being the result of Compton scattering of synchrotron photons by high-energy electrons. This estimate is based on the fact that the ratio of intensities of synchrotron and (inverse) Compton emission by high-energy electrons is equal to the ratio of densities of photon and magnetic fields. Knowing the size of the nebula, one could readily estimate the energy density of the synchrotron photons there and derive an estimate of magnetic field $B \sim 10^{-4}$ G. This estimate leads to the estimate of maximal energies of electrons in the nebula, $E_e \sim 10^{16}$ eV.

### 4.3.1 Particle acceleration in pulsar magnetosphere

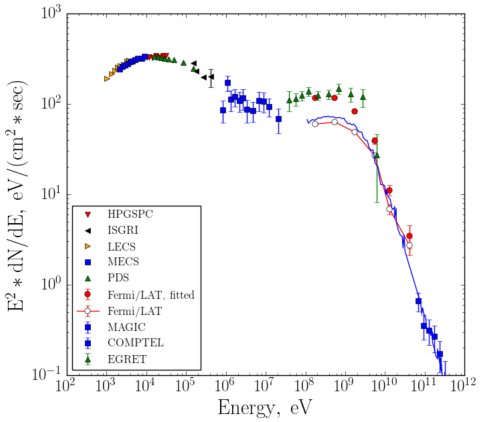


Figure 4.3.2: Spectrum of pulsed emission from Crab pulsar.

Emission from the direct vicinity of the neutron star could be separated from the larger scale nebula emission based on the pulsed nature of the near-neutron-star signal. The spectrum of pulsed emission from Crab extends up to 100 GeV band and beyond, see Fig. 4.3.2. This means that electrons are (at least initially) accelerated close to the neutron star.

As it is mentionned above, the neutron star possesses an extremely high magnetic field, $B \sim 10^{12}$ G. Motion of particles in the direction transverse to the magnetic field is suppressed because of severe synchrotron loss. Electrons have velocities approximately aligned with magnetic field lines. In such situation the "minimal" energy loss which the high-energy particles could not escape is the loss on the so-called "curvature" radiation. The magnetic fields of the dipole have curvature radius

of the order of the typical size scale of the system (say, about the distance to the neutron star). A charged particle moving along a trajectory with curvature radius $R$ emits electromagnetic radiation quanta with characteristic energy

$$E_{\rm cur} \sim \frac{E^3}{Rm^3} \simeq 10^{11} \left(\frac{m}{m_e}\right)^{-3} \left[\frac{E}{10^{13}\ {\rm eV}}\right]^3 \left[\frac{R}{10^6\ {\rm cm}}\right]^{-1}\ {\rm eV} \tag{4.3.2}$$

If the observed high-energy emission is interpreted as curvature radiation, observations of pulsed emission in the energy band $\sim 100$ GeV suggests that electrons are accelerated up to the energies at least $\sim 10$ TeV near the pulsar. Alternatively, the high-energy component of the pulsed emission could be produced via Compton up-scattering of lower energy photons (e.g. of the $\epsilon \sim 1$ keV energy photons forming the lower energy "bump" in the pulsed emission spectrum in Fig. 4.3.2. Still, even in this case, the energy of the up-sattered photons is

$$E_{IC} \sim \min\left(E_e, (E_e/m_e)^2\epsilon\right) \tag{4.3.3}$$

Pulsed emission at several hundred GeV is produced by electrons with energies not less than several hundred GeV.

Charged particles could be accelerated by electric field which should have a non-zero component along the particle velocity. Since particles are bound to spiral along magnetic field lines, the condition for particle acceleration is the presence of non-zero electric field component along the magnetic field field lines or

$$(\vec{E}\cdot\vec{B}) \neq 0 \tag{4.3.4}$$

Non-zero electric field around the magnetized neutron star is created in result of the star rotation. To understand this effect one has to consider the surface layer of the neutron star which in which free protons and electrons (and a certain amount of heavier atomic nuclei). Electrons and protons corotate with the neutron star with velocity $v_\phi = \Omega R\sin\theta$ where $\theta$ is the angle between the particle radius vector and rotation axis and $\Omega = 2\pi/P$ is the angular velocity of the neutron star. The magnetic dipole field just outside the surface of the neutron star is

$$\begin{aligned} B_r &= \frac{2B_0R^3}{r^3}\cos\theta \\ B_\theta &= \frac{B_0R^3}{r^3}\sin\theta \end{aligned} \tag{4.3.5}$$

(we assume for simplicity that the magnetic dipole moment is aligned with the rotation axis). This field produces a Lorentz force on the particles. This force has a component along the neutron star surface

$$F_\theta = ev_\phi B_r = 2eB_0\Omega\cos\theta\sin\theta \tag{4.3.6}$$

which pushes electrons to move versus the North / South magnetic poles while pushing protons to move toward the equator or vise versa, depending on the sign of the magnetic moment.

This leads to charge separation in the form of overdensity of electrons in the pole regions and overdensity of protons in the equatorial region or vise versa. Charge separation, in turn, leads to the creation of electrostatic electric field. Electric field component parallel to the neutron star surface could be found from the condition of exact compensation of the initial Lorentz force by the electrostatic force due to the charge re-distribution

$$E_\theta = -v_\phi B_r = 2B_0\Omega\cos\theta\sin\theta \tag{4.3.7}$$

Vacuum solution of Maxwell equations outside the neutron star with the boundary condition (4.3.7) for the $\theta$ component of electric field at the sphere with radius $R$ has the form

$$\vec{E} = \nabla\Phi, \quad \Phi = -\frac{B_0R^5\Omega}{6r^3}(3\cos^2\theta - 1) \tag{4.3.8}$$

Consider, for example the magnetic and electric fields at the rotatin axis. The magnetic field is radial at the axis. The radial component of electric field is not zero and

$$E_rB_r = \frac{\partial\Phi}{\partial r}B_r \sim \frac{B_0^2R^8\Omega}{r^7} \neq 0 \tag{4.3.9}$$

The potential difference between the poles and infinity is

$$U = (\Phi(R) - \Phi(\infty)) = B_0R^2/\Omega/3 \simeq 2\times10^{19}\left[\frac{B}{10^{12}\text{ eV}}\right]\left[\frac{P}{1\text{ ms}}\right]^{-1}\text{ V} \tag{4.3.10}$$

Thus, electrostatic field produced by the charge redistribution induced by rotation of the neutron star could accelerate particles in the vicinity of the pulsar to extremely large energies.

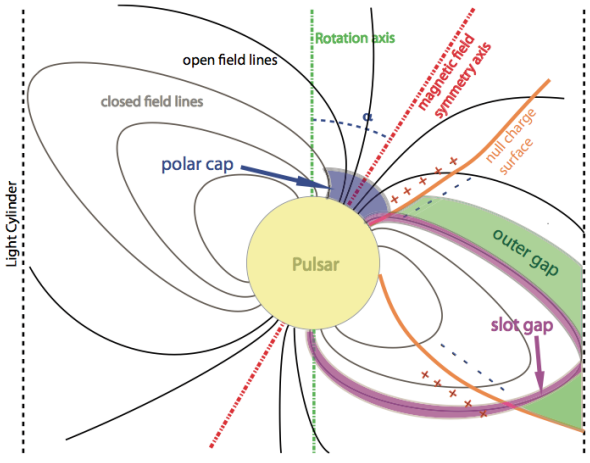


Figure 4.3.3: Possible locations of particle acceleration regions ("vacuum gaps") in pulsar magnetosphere

In fact, the extreme energies (4.3.10) could never be attained in reality. The problem is that vacuum which might (hypothetically) exist around neutron star is unstable with respect to various pair creation processes. Pair production initiates development of electromagnetic cascade in the direct vicinity of neutron star. This cascade leads to the deposition of a large amount of $e^+e^-$ pairs. At sufficiently high pair plasma density, charge redistribution will lead to the neutralization of the accelerating component of electric field and formation of the so-called "force-free" magnetosphere, i.e. plasma distribution in which the net Lorentz force vanishes everywhere:

$$\vec{E} + \vec{v}\times\vec{B} = 0. \tag{4.3.11}$$

The force-free magnetosphere could be maintained only if $e^+e^-$ pairs are continuously supplied to the space around the pulsar. The problem is that plasma which could freely

move along the magnetic field lines is continuously "washed out" from the magnetosphere (together with electromagnetic field) by the centrifugal force. Continuous supply of the plasma could be provided only be the pair produciton process. The pair production process could work only if there are high-energy particles producing sufficiently high energy gamma quanta. This means that high-energy particles have to be continuously produced at some (as for now, uncertain) locations in the magnetosphere. These particle acceleration sites are called "vacuum gaps" (in the sense that particle acceleration in the gaps is similar to the particle acceleration in the vacuum case considered above). Possible locations of the magnetospheric vacuum gaps are shown in Fig. 4.3.3. Different possible gap locations imply slightly different pair production thresholds for the curvature $\gamma$ quanta.

# Chapter 5

# Black holes and active galactic nuclei

## 5.1 Stellar mass black holes

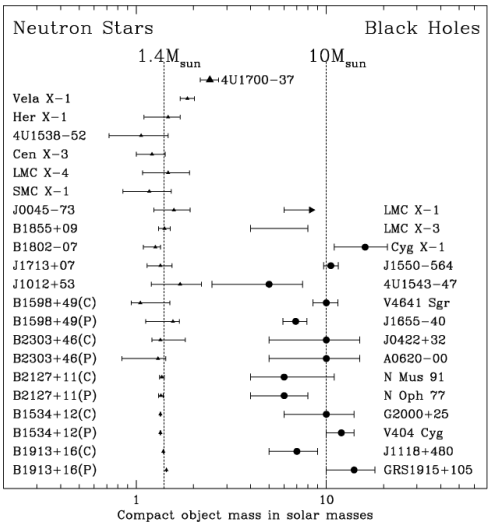


Figure 5.1.1: Masses of compact objects in X-ray binary systems. Objects of the masses above $3M_\odot$ are black holes.

The hydrostatic equilibrium of the neutron star is supported by the pressure of neutron matter. Similarly to the degenerate electron gas in the iron core of a massive star, the pressure of the degenerate neutron gas could counteract gravity only as long as it is non-relativistic. From Fig. 4.2.4 one could see that stability of the neutron gas is lost at about $2.7M_\odot$. If the neutron star accumulates more than this mass during the gravitational collapse of the parent massive star, the collapse process will not end at the neutron star configuration, but instead will proceed toward a more compact configuration.

We do not know any forms of matter which could be more compact that the nuclear matter inside the neutron stars. In fact, there is no known state of matter which would have pressure strong enough to resist the gravity in the configuration with the size smaller than $\sim 10$ km and mass $\geq 3M_\odot$. The simplest possible assumption is that the end stage of the gravitational collapse will be a black hole.

First "traces" of the stellar mass black holes were revealed with the start of the X-ray astronomy. An unexpected discovery of the first X-ray telescopes (initially constructed to study extremely weak X-ray emission from normal stars like the Sun) was the detection of bright X-ray sources with luminosities reaching $\sim 10^5 L_\odot$. Soon after the discovery, it became clear that the X-ray emission originates from stellar binary systems, with only one of the companion stars visible in the optical band, while the other emitting in the X-rays. The X-ray luminosity of the optically invisible star, is at the level of Eddington luminosity

$$L_{Edd} = \frac{4\pi G M m_p}{\sigma_T} \simeq 10^{38} \left[\frac{M}{M_\odot}\right] \text{ erg/s} \qquad (5.1.1)$$

This luminosity is the maximal possible luminosity at which the radiation pressure force (acting on electrons) $f_{rad} \simeq L_{Edd}\sigma_T/4\pi R^2$ ($L_{Edd}/4\pi cR^2$ is the energy density of radiation contained within a region of the size $R$) balances the gravitational force (which is stronger for protons) $f_{grav} = GMm_p/R^2$. Expression for $L_{Edd}$ is obtained from $f_{grav} \sim f_{rad}$.

The temperature of the system accreting at the Eddington rate is related to its size: $L_{Edd} = 4\pi R^2 T^4$. The fact that the temperature is in X-ray range implies that the object is very compact:

$$T \simeq \frac{L_{Edd}^{1/4}}{R^{1/2}} \simeq 5 \left[\frac{M}{M_\odot}\right]^{1/4} \left[\frac{R}{10 \text{ km}}\right]^{-1/2} \text{ keV} \tag{5.1.2}$$

Thus, the X-ray emitting component of the binary system has to be a compact star with mass about the solar mass and size about the neutron star size. Measurements of the periodic variations of the radial velocity of the visible component of the X-ray binary allow to determine the dynamical parametes of the system and measure the mass of the compact object. Fig. 5.1.1 shows the results of such measurements in a number of X-ray binaries. One could see that the binaries are divided onto two types. In a significant fraction of the binaries the mass of the compact object is close to the Chandrasekhar mass, which indicates that the compact object is most probably the neutron star. At the same time, in some binaries the mass of the compact object is larger than $\sim 3M_\odot$, a theoretical limit of stability of neutron stars. The compact objects in these binaries are most probably black holes.

Dissipation of liberated gravitational energy of matter falling into gravitational potential well of a black hole is one of the most efficient mechanisms of extraction of energy from matter. Indeed, the total energy potentially extractable from a particle of the mass $m$ is its rest energy, $E = m$. Consider a particle orbiting a black hole on a Keplerian orbit at a distance $r$. The gravitational energy which needs to be released by the particle to settle at this Kelperian orbit is $U = GM_{BH}m/r$, where $M_{BH}$ is the black hole mass. This energy could be released radiatively, when the accretion flow compresses and heats up while approaching the black hole. By the time when particles reach the distance of the innermost stable circular orbit situated at $6\times$ the gravitational radius,

$$R_{isco} = 6R_g \sim GM_{BH} \simeq 10^2 \left[\frac{M_{BH}}{10M_\odot}\right] \text{ km} \tag{5.1.3}$$

the released gravitational energy per particle reaches the value $U \sim GM_{BH}m_p/R_{isco} \sim 0.1m_p$, i.e. it becomes a sizeable fraction of the total rest energy of the particle. Detailed calculations based on General Relativity show that the efficiency of extraction of the rest energy of accretion flow depends on the rotation moment of the black hole. Matter approaching the innermost stable ciccular orbit around non-rotating black holes could convert $\simeq 10\%$ of the rest energy into radiation. The innermost stable circular orbit around maximally rotating black holes (those for which the horizon surface rotates with the speed of light) approach closer to $R_g$ and the liberated gravitational energy constitutes 40% of the rest energy of the accreting matter.

## 5.2 Observable relativistic gravity effects

Black holes provide useful laboratory for the study of relativistic gravity (not possible in Earth-bound laboratory conditions). Relativistic gravity related effects have to be singled out in the imaging, timing and spectral characteristics of emission from the innermost part of the accretion flow close to the black hole horizon.

Emission from this part of the accretion flow could be singled out based on its extremely fast variability. The frequency of circular orbits around black holes scales with the distance $r$ as

$$\nu \sim \frac{(GM)^{1/2}}{2\pi r^{3/2}} \sim 0.2 \left[\frac{10M_\odot}{M}\right] \left[\frac{r}{6GM}\right]^{-3/2} \text{ kHz} \qquad (5.2.1)$$

The phenomenon of milli-second variability of emission from X-ray binaries is studied in the form of kHx Quasi-Periodic Oscillations (QPO).

**Problem.** Nearby Galactic X-ray binaries emitting at Eddington luminosity produce flux at the level of $F \sim 10^{-10}$ erg/(cm$^2$s) in X-rays (photon energies above keV). Find the effective collection area of an X-ray telescope necessary for the study of details of variability of X-ray emission at the time scale of the period of rotation around the innermost stable circular orbit around stellar mass black hole.

A bright blob orbiting along more-or-less stable circular orbit for sufficiently long time produces quasi-periodic signal. Periodicities appear as peaks in the power spectrum (Fourier transform of the time series) of the source at the frequencies corresponding to the periodicities present in the signal.

An example of the QPOs in a Galactic black hole candidate GRS 1915+105 is shown in Fig. 5.2.1. QPOs most of the time come "in pairs" with the frequencies of the pair having ratio of about 3:2. The origin of this 3:2 pairs is not clear. Several possible explanations are under the discussion. For the black hole candidates the most common model is that one of the frequencies is just the frequency of rotation around the nearly circular orbit, while the other one reflects the deviations from the circularity (the known effect of precession of the perihelion of the nearly elliptic orbit or Lense-Thirring precession of the orbital plane). Next generation X-ray telescopes with large collection area, like ESA mission Athena and Chinese-led X-ray telescope XTP with collection area 3.5 m$^2$, see Fig. 5.2.2, will provide more details on the phenomenon. The Large Area Detector of eXTP will be a set of deployable panels made of Silicon Drift Detectors with micro-collimator tubes.

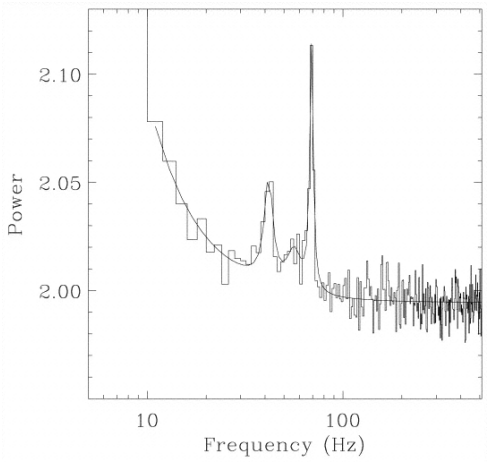


Figure 5.2.1: High-frequency quasi-periodic oscillaitons in the micro-quasar GRS 1915+105.

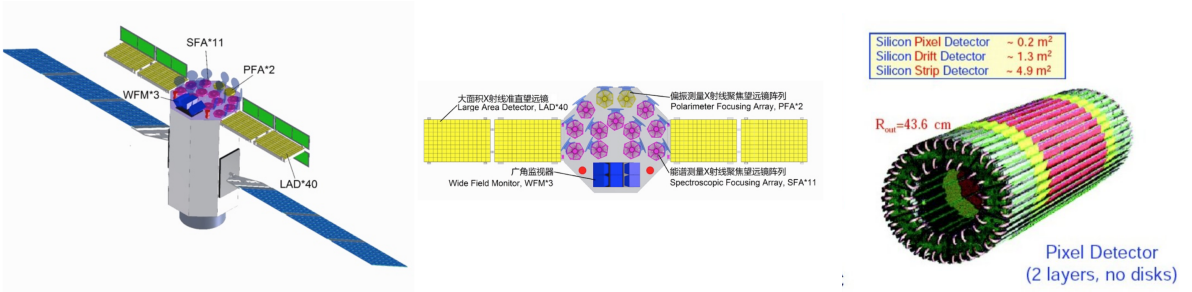


Figure 5.2.2: Next-generation X-ray telescope eXTP. Yellow panels show Large Area Detector, based on Silicon Drift Detector technology. For comparison, right panel shows the tracker of ALICE / LHC which also includes Silicon Drift Detector.

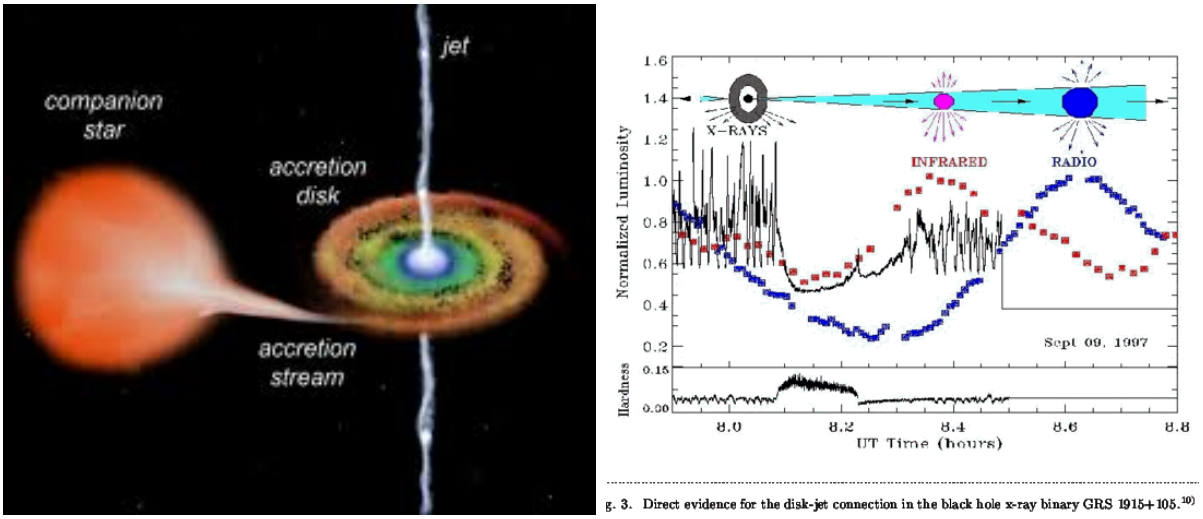


Figure 5.2.3: Left: accretion disk-jet structure of black hole powered X-ray binaries. Right: evolution of the X-ray, infrared and radio fluxes at the moments of matter ejection into the jet of X-ray binary GRS 1915+105.

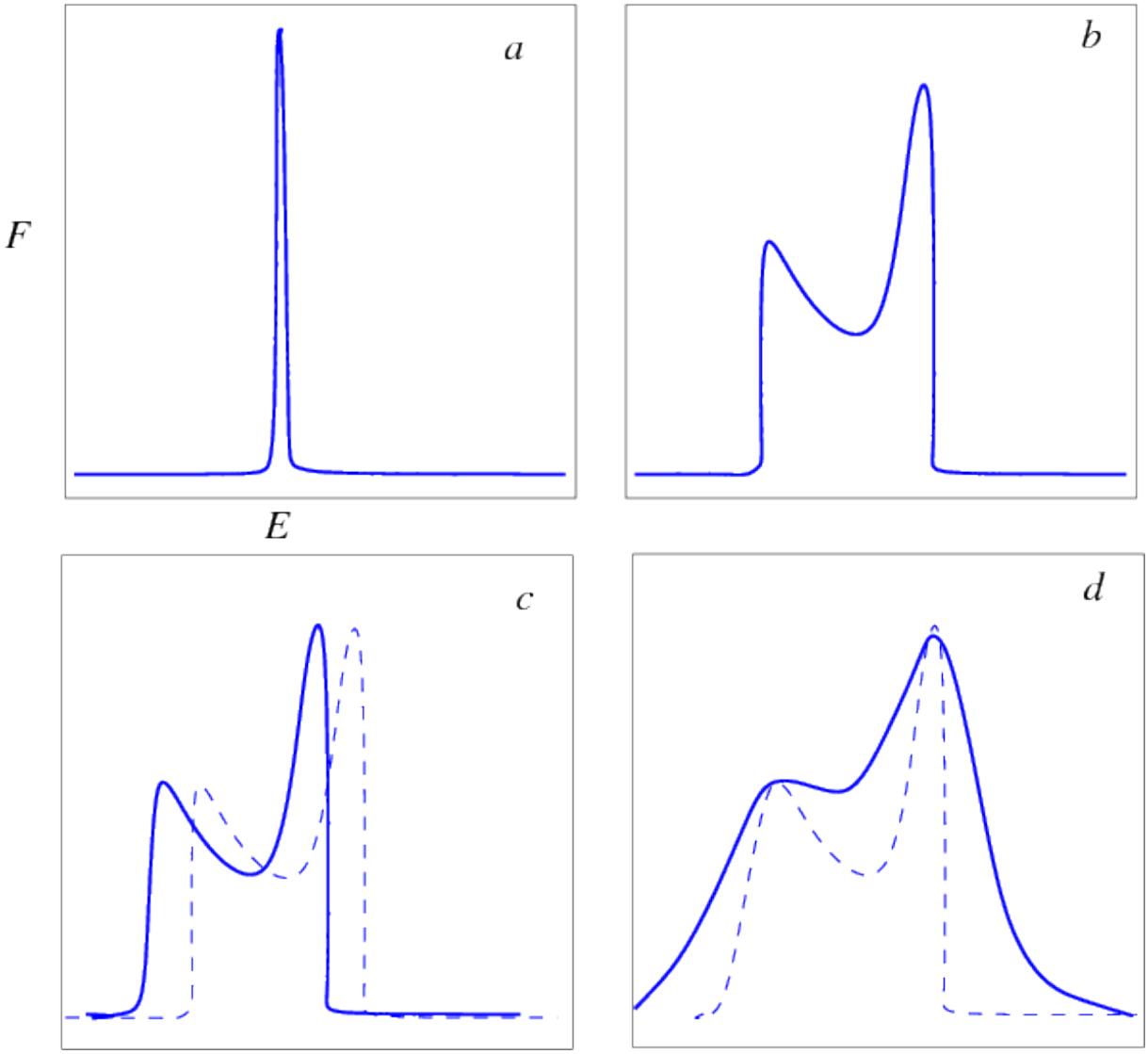


Figure 5.2.4: Qualitative representation of the influence of Doppler and General Relativistic effects on the iron line.

Another manifestation of relativistic gravity effects in the observational data is in the form of relativistically broadened atomic emission lines. Qualitatively the Doppler effect and the effects of General Relativity affect the lines as it is shown in Fig. 5.2.4.

Doppler effect leads to the appearance of a double peaked structure of the line *(b)*. The blue-shifted "wing" of the line comes from the part of the disk which moves toward an observer. The red-shifted wing is from the part moving away from the observer. The blue-shifted part appears brighter because of the "relativistic boosting" of the flux, $F \sim \Gamma^3$ ($\Gamma$ is the bulk Lorentz factor). Gravitational red-shift factor $g$ near the horizon shifts the line to lower energies *(c)*. Finally, the lines produced by the rings orbiting the black hole at different distances add together and produce a "smoothed" averaged profile, shown in Fig. 5.2.4*d*.This effect is observed in the spectra of X-ray binaries which emit a fluorescence line produced by ionised iron nuclei in the keV range (6.4 keV). This line is sometimes

observed extremely broadened to $\Delta E/E \sim 1$.

Black holes in X-ray binaries produce episodically (via an uncertain mechanism) jet-like outflows (Fig. 5.2.3). During the jet-ejection episodes, blobs of plasma filled with high-energy electrons are ejected in one and the same direction (presumably along the black hole rotation axis). Synchrotron emission produced by the high-energy electrons could be detected from the jets up to parsec-scale distances (distance scale some 10 orders of magnitude larger than the size of the black hole).

Binary systems with two massive stars are short-lived (each star leaves some 1-100 Myr, much shorter than the e.g. the Sun). Each star of the binary finally ends its life in a core collapse resulting in formation of either black hole or a neutron star. A small fraction of those systems in which one star has already exploded, but the other has not yet, are observed as High Mass X-ray binary systems. The fate of such systems is formation of binary neutron star, black hole + neutron star and binary black hole systems. Binary black hole systems are remarkably difficult to observe because there is no matter left around the black holes and these systems could not be powered by accretion. First explicit observation of a binary black hole system was done in 2016 with the help of a gravitational wave detector Advanced LIGO, which has detected an event of merger of two black holes in a binary system. The gravitational wave signal of this merger event, GW150914, is shown in Fig. 5.2.5.

Within the General Relativity description of relativistic gravity, the gravitational radiation is quadrupole, with luminosity

$$L_{GW} = \frac{1}{5} G_N \langle \dddot{I}_{jk} \dddot{I}_{jk} \rangle \tag{5.2.2}$$

proportional to the third time derivative of the quadrupole moment of the mass distribution. For a binary system with companion object masses $M_1 \simeq M_2 \simeq M$ and binary separation $r$, $I \sim Mr^2$ and its third time derivative is proportional to the orbital angular frequency

$$\Omega = \sqrt{\frac{GM}{r^3}} \tag{5.2.3}$$

in the third power: $\dddot{I} \sim \Omega^3 M R^2$. This gives

$$L_{GW} \simeq G\Omega^6 M^2 r^4 \simeq \frac{G^4 M^5}{r^5} \simeq 10^{51} \left[\frac{r}{10^8 \text{ cm}}\right]^{-5} \left[\frac{M}{10^{34} \text{ g}}\right]^5 \text{ erg/s} \tag{5.2.4}$$

At the same time, total gravitational energy which could be released by a merger of companions is a fraction of the rest energy of the two bodies:

$$E_{grav} = \frac{GM^2}{r} \lesssim M \sim 10^{55} \left[\frac{M}{10^{34} \text{ g}}\right] \text{ erg} \tag{5.2.5}$$

A close binary composed of two stellar mass black holes with separation just about 10-100 times the size of the black hole horizon would loose all its energy onto gravitational radiation on an hour time scale. A binary with the orbital separation $10^3$ times larger looses energy via gravitational radiation on the time scale comparable to the age of the Universe. The the black holes merged in the GW150914 event should have formed a very close binary system.

The final stage of the merger occurred when the binary separation was about the gravitational radius of the black holes, $r \sim GM$. The characteristic time scale of this final stage is

$$t \sim \frac{E_{grav}}{L_{GW}} \simeq \frac{r^4}{G^3 M^3} \gtrsim r \sim 1 \text{ ms} \qquad (5.2.6)$$

This is the time scale of the fastest and strongest amplitude oscillations of the signal in Fig. 5.2.5.

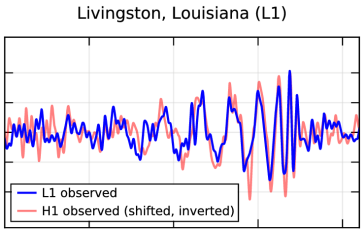


Figure 5.2.5: Gravitational wave signal from a binary black hole merger GW150914.

### 5.2.1 Active galactic nuclei.

Compact sources of radio-to-$\gamma$-ray emission are found in the centers of certain types of galaxies. These sources are called radio-loud "active galactic nuclei" (AGN). Measurements of the electromagnetic fluxes of AGN indicate that their luminosities reach the level of $> 10^{45}$ erg/s, i.e. larger than typical luminosity of the Milky Way type galaxies. Due to their extremely high luminosities, the brightest AGN have observational appearance similar to stars in the visible band. Based on this appearance, certain type of the bright AGN has been called "Quasars", for "quasi-stellar" objects.

Study of variability of emission from AGN reveals variability time scales down to days, hours and sometimes even minutes and seconds. This implies that the variable emission comes from a compact region of the size $R \leq ct_{var} \sim 1\,[t_{var}/10 \text{ min}]$ AU. Such enormous energy output, equivalent to $10^{12}$ Suns, could not be produced by a compact stellar cluster confined to the region of the size of the order of the distance from the Earth to the Sun. Similarly to the case of X-ray sources in binary systems, the only reasonable energy reservoir which could power AGN is thought to be gravitational energy of matter accreting on a compact region.

Re-applying the formula for the Eddington luminosity (5.1.1) to AGN one finds that the mass of the object onto which matter accretes should be at least $10^7 M_\odot$ to provide the power at the level of $10^{45}$ erg/s. The estimate of the mass of the compact object in the AGN "central engine" is often obtained also from the study of statistics of AGN observations. This study shows that the observed number of AGNs could be explained if the lifetime of these sources in the nuclei of galaxies is $T_{AGN} \sim 10^7 - 10^8$ yr. If the source produces luminosity at the level of $L_{AGN} \sim 10^{45}$ erg/s over this time span, the total energy output of the source is $E_{AGN} \sim L_{AGN} T_{AGN} \sim 10^{60}$ erg. Assuming the best possible efficiency of conversion of the energy of the rest energy of the "fuel" which powers the AGN into radiation, $\sim 10\%$, we could find that the mass of the "waste" which should be left by the AGN activity is $M \geq 10 E_{AGN}/c^2 \sim 10^7 M_\odot$. This mass should reside somewhere in the source, so it is presumably confined within the region of the size $\sim 1$ AU, found from the variability time scale. Comparing this size to the gravitational radius of a $10^7 M_\odot$ body (5.1.3), we find that all the mass is, in fact contained in the region of the size comparable to the size of a $10^7 M_\odot$ black hole. Based on this observation, the most common hypothesis is that the objects powering the AGN are "supermassive" black holes.

The range of phenomena associated to the supermassive black holes is similar to the phenomena observed in the stellar mass black holes (the term "microquasars" is sometimes used for the black hole powered X-ray binary stellar systems). Estimating the temperature of accretion flow onto the supermassive black hole from Eq. (5.1.2) one finds that for the supermassive black holes

$$T \simeq \frac{L_{Edd}^{1/4}}{R_g^{1/2}} \sim 100 \left[\frac{M_{BH}}{10^7 M_\odot}\right]^{-1/4} \text{ eV} \qquad (5.2.7)$$

is expected to be in the UV range. such (quasi)thermal radiation form the accretion flow is observed in the form of "Big Blue Bump" in the spectra of quasars (see Fig. 5.2.6, the Big Blue Bump is visible in the lower panel of the figure, in the frequency range $\sim 10^{15} - 10^{16}$ eV).

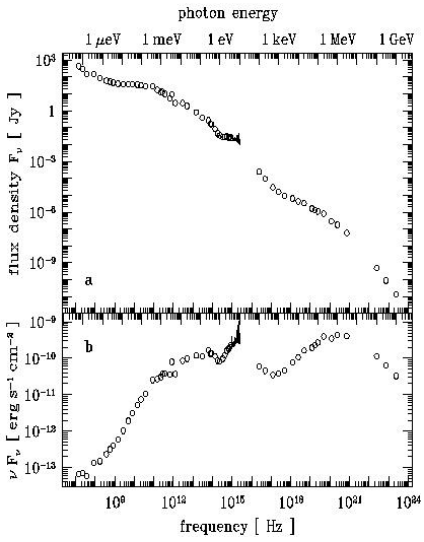


Figure 5.2.6: Broad band spectrum of a quasar 3C 273.

Radio-loud AGN produce jet-like outflows which, contrary to the jets of the stellar mass black holes are generated steadily, rather than episodically, by the AGN central engines. The jets extend up to the 100 kpc – Mpc distance scales (again, ten orders of magnitude larger than the size of the black hole) and originate directly from the supermassive black hole. Large size of the supermassive black holes enables direct imaging observations of the jets at the distance scales as short as the gravitational radius of the black hole in the case of the nearest and largest supermassive black holes.

The best studied example is the jet of the nearby "radio-loud" AGN M87, which is found in the nucleus of a giant elliptical galaxy in the center of the nearest-to-us galaxy cluster Virgo. The radio image of the M87 jet is shown in Fig. 5.2.7, Due to its proximity, the optical emission from the jet is visible already with moderate power telescopes. The M87 jet was discovered in the visible light back in 1919, almost hundred years ago.

The black hole mass in M87 is in the range $\sim 3 \times 10^9 M_\odot$, so that the size of the black hole horizon is $\sim 10^{15}$ cm. At the distance 16 Mpc, the angular size of the supermassive black hole in the nucleus of M87 is $\theta = 10^{15}$ cm$/16 \times 3 \times 10^{24}$ cm$\sim 4$ $\mu$as. To resolve the region of the size about the size of the black hole horizon, a telescope with angular resolution in the micro-arcsecond range is required. Contours in Fig. 5.2.7 show the image of the core of M87 taken with the Very Large Baseline Array (VLBA) radio telescope, which is a network of radio

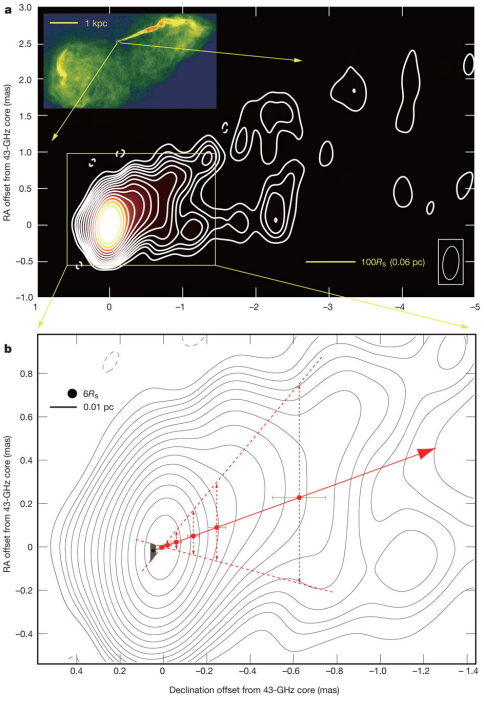


Figure 5.2.7: Radio jet of the galaxy M87 on different distance scales.

antennae working as a single telescope with aperture equal to the distance between the telescopes. This allows to achieve angular resolution in the range $\theta_{resolution} \sim \lambda/D \sim 0.1 - 1$ mas, where $\lambda$ is the wavelength of the radio signal and $D$ is the distance between the telescopes. From Fig. 5.2.7 one could see that the M87 jet originates from the region of the size not larger than $\simeq 10$ the black hole horizon size. The jet launch point has recently been resolved with Very-Long Baseline Interferometry technique in sub-mm wavelength range. The region of jet launch is found to be contained within the so-called "innermost stable circular orbit" around the M87 black hole.

Similarly to the jets of the stellar mass black holes, the jets of the supermassive black holes are filled with high-energy electrons. In the particular case of the M87 jet, observations of the synchrotron emission from the jet electrons indicate that electron energies reach some 100 TeV. Thus, either the AGN central engine, the supermassive black hole, or the jet itself work as powerful particle accelerators.

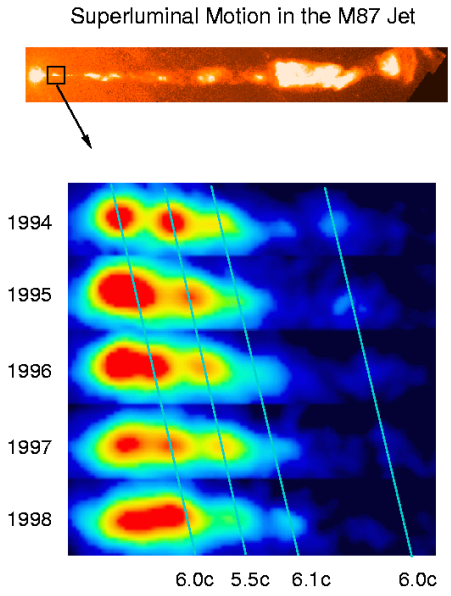


Figure 5.2.8: Superluminal motion of the blobs of the M87 jet.

Systematic re-observation of AGN jets on the time scales of years shows that the jets are dynamic structures, with bright "blobs" moving away from the AGN "central engine". In fact, the measured speeds of the jet blobs often exceed the speed of light (see Fig. 5.2.8). This effect is not related to the real superluminal motion, but is an artifact of projection and Doppler effects. The Doppler effect is also responsible for the one-sided appearance of the M87 jet evident from Fig. 5.2.7.

### 5.2.2 Supermassive black hole in the Milky Way.

The best studied supermassive black hole in galactic nucleus is the Milky Way supermassive black hole. It is situated in the source in the contellarion of Sagittarius, called Sgr A*. Image of this source in the radio band is shown in Fig. 5.2.9.

The center of the Milky Way is situated at the distance $\simeq 8$ kpc away from the Sun. In the visible band it obscured by the dust filling the Galactic Disk. However, stars in the Galactic Center region are visible in the infrared band. The source Sgr A* itself is most of the time not visible in the infrared, except for the flaring periods of increased activity. Observations of motion of the stars in the region around Sgr A* show that they move along elliptical orbits (Fig. **??**). The periastron of the closest approaching orbit is just $\sim 10^{15}$ cm (100 AU) away from Sgr A*. Dynamics of the orbits is consistent with motion around a central point object of the mass $M_{BH} = 4 \times 10^6 M_\odot$. The most straightforward model for the compact central object is that it is a supermassive black hole.

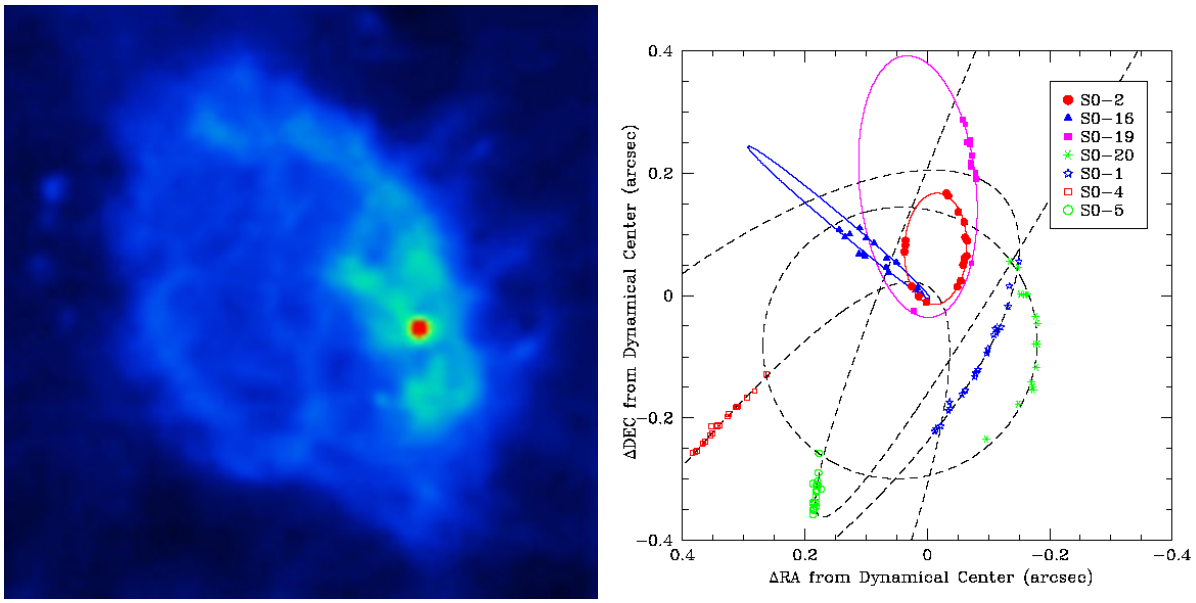


Figure 5.2.9: Image of the source Sgr A* (red) hosting the supermassive black hole of the Milky Way galaxy. Blue bubble-like structure around the source is Sgr A shell of the size $\sim 10$ pc. Right: Stellrar orbits around Sgr A*.

The angular size of the supermassive black hole in the Milky Way center could be calculated similarly to the size of the M87 black hole. This gives some $\sim 20$ $\mu$as. The required angular resolution was, in fact, already reached by the radio telescopes using the technique of very-long-baseline interferometry. First constraints on the size of the radio source in Sgr A* obtained with this technique indicate that the radio emission originates directly from the black hole horizon.

# Appendix A

# Natural system of units

Units of measurement used in astrophysics are often very different from those commonly used in the particle physics (and from the SI, the International System of units which you used in school). To facilitate comparison between astrophysical and high-energy physics quantities, astroparticle physics often uses the so-called "Natural" system of units.

The idea behind these Natural Units is to reduce the number of different units which measure in essence one and the same quantity. For example, the temperature is a measure of the typical kinetic energy of random motions of molecules, so there is no reason why it should be measured in separate units, (e.g. in Kelvin), rather than in the units of energy. Since Kelvin units are introduced through a constant renormalization of the energy, $E \sim k_B T$, by the Boltzmann constant $k_B$, one could simply choose units in which $k_B = 1$ so that in the new units the units of the temperature are just the same as the units of energy, $E \sim T$.

In a similar way, one could relate the units of energy to the units of time. One could use photons for this: for each photon frequency (i.e. inverse time) there is a well defined energy, so that it makes no difference if one talks about frequency or the energy of a photon. Choosing the units in which

$$\hbar = 6.6 \times 10^{-16} \text{ eV s} = 1 \tag{A.0.1}$$

one could measure the frequency in the units of energy, so that the equation $E = \hbar\omega$ for the photon energy reads $E = \omega$. The conversion rule from energy to time units is then

$$1 \text{ eV} \equiv \frac{1}{6.6 \times 10^{-16} \text{ s}} \tag{A.0.2}$$

Finally, the units of energy/time could be used to measure the distance also. Indeed, the photon wavelength is unambiguously related to its frequency or energy via the relations $\nu = c/\lambda$ and $E = 2\pi\hbar c/\lambda$. Thus, fixing

$$c = 3 \times 10^{10} \text{cm/s} = 1 \tag{A.0.3}$$

The conversion between eV, s and cm is then

$$1 \text{ eV} \equiv \frac{1}{6.6 \times 10^{-16} \text{s} \cdot 3 \times 10^{10} \text{cm/s}} \simeq \frac{1}{2 \times 10^{-5} \text{ cm}}, \quad 1 \text{ s} \equiv 3 \times 10^{10} \text{ cm} \tag{A.0.4}$$

The relation (A.0.3) implies still further reduction of the number of independent units. In particular, the mass could be measured in the energy, time or distance units, because the relation $E = mc^2$ becomes just $E = m$, so that the units of mass are the same as the units of energy. The conversion coefficient could be found based on the known mass and rest energy of e.g. electron:

$$m_e = 9 \times 10^{-28}\ \text{g} = m_e c^2 = 5 \times 10^5\ \text{eV} = \frac{m_e c}{\hbar} = \frac{1}{4 \times 10^{-11}\ \text{cm}} \tag{A.0.5}$$

In fact, the distance scale associated to a given mass scale in the Natural system of units is the Compton wavelength of a particle of mass $m$.

Electric charge is a dimensionless quantity, as one could see from the expression for the fine structure constant

$$\alpha = \frac{e^2}{\hbar c} = \frac{1}{137.04} \to e = \sqrt{\frac{1}{137}} \simeq 0.085 \tag{A.0.6}$$

The magnetic and electric permeability of vacuum introduced in the SI system could be fixed to $4\pi\epsilon_0 = 4\pi\mu_0 \equiv 1$. After such a simplification the Coulomb law becomes

$$F = \frac{q_1 q_2}{r^2} \tag{A.0.7}$$

The units of measurement of magnetic fields are the square of the energy unit:

$$\begin{aligned} 1\ \text{T} = 10^4\ \text{G} = 1\frac{\text{V s}}{\text{m}^2} &= \frac{1\text{eV}}{e}\frac{3 \times 10^{10}\ \text{cm/s} \cdot 1\ \text{s}}{10^4\ \text{cm}^2} \\ = 3 \times 10^7\ \text{eV} \cdot \frac{2 \times 10^{-5}\ \text{eV cm}}{\text{cm}} &\quad \to \quad 1\ \text{G} \simeq 7 \times 10^{-2}\ \text{eV}^2 \end{aligned} \tag{A.0.8}$$

Electric and magnetic fields are just different components of one and the same tensor of electromagnetic field, so that they are obviously measured in the same units.

| | |
|---|---|
| **Problem A.1** | Find the value of the Gravitational constant $G_N$ in the Natural System of units. What is the dimension of $G_N$? Based on the dimension of $G_N$, associate the distance/energy/time scale associated to $G_N$. Find characteristic distance scale associated to a gravitating body of the mass $M$. Find the value of the mass $M$ at which such characteristic "gravitational" distance scale becomes comparable to the Compton wavelength of a particle of mass $M$. |

| | |
|---|---|
| **Problem A.2** | Find the strength of magnetic field (Schwinger magnetic field) at which the motion of electron in magnetic field becomes quantized (the gyroradius becomes equal to the Compton wavelength). Compare this strength with the strength of magnetic field (a) at the surface of the Earth (b) with the fields in excess of $B \sim 10^{12}$ G found near neutron stars. |

# Bibliography

[1] Planck Collaboration, Ade, P. A. R., Aghanim, N., et al. 2015, arXiv:1502.01589